FACULTY OF SCIENCES

A new ray tracing algorithm for complex ice models and the analysis of ice properties using weather balloons

Arthur Adriaens

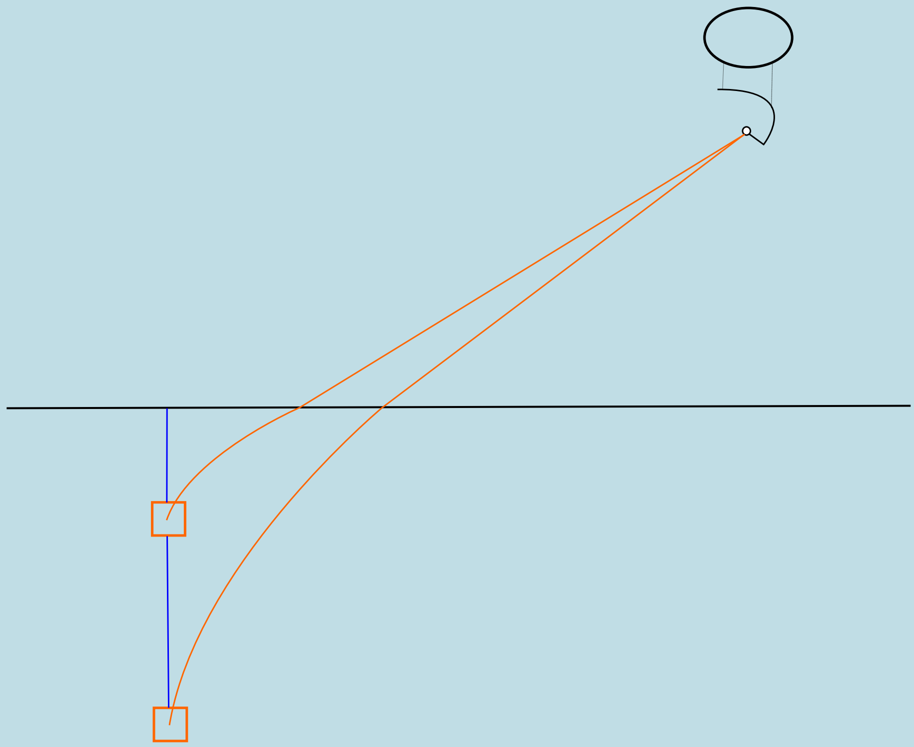

Department of Physics and Astronomy

Promotor: Prof. dr. Dirk Ryckbosch Dirk.Ryckbosch@ugent.be

Accompanist: Bob Oeyen Bob.Oeyen@ugent.be

Master's dissertation submitted in partial fulfilment of the requirements for the degree of master in Physics and Astronomy

GHENT UNIVERSITY

ABSTRACT

The Radio Neutrino Observatory in Greenland - RNO-G - is under construction at Summit Station in Greenland to search for neutrinos of several PeV energy up to the Eev range. It's a mid-scale, discovery phase, extremely high-energy neutrino telescope that will probe the astrophysical neutrino flux at energies beyond the reach of IceCube. More particularly if will make it possible to reach the next major milestone in astroparticle physics: the discovery of cosmogenic neutrinos. All simulations carried out within this work were made with the three

programs

- NuRadioMC
- radiotools
- RadioPropa

whom are free to download on github. This masters thesis consists of three major parts, first off a background is given on what neutrinos are and how the detector works, these are chapters 2-4, then chapter 5 explains how a new algorithm called the *Hybrid minimizer* was built. This is an algorithm for finding the path(s) of a radio source (e.g a neutrino interaction) to the detector in complex ice models. And lastly, in chapter 6 it's explained how an indirect measurement was done of the index of refraction around the deep components of the detector using both weather balloon gps data and detector responses. All the code for both the simulations carried out throughout this thesis as well as the testing of the algorithm that was built can be found here, the algorithm itself can be found here within the branch radiopropa/hybrid_minimizer.

VOORWOORD

De *Radio Neutrino Observatory in Greenland* - RNO-G - is een detector die momenteel onder constructie is in Groenland. Deze detector heeft als doel het vinden van neutrinos met energieën van enkele PeV tot in het EeV gebied. Deze extreem hoge energie neutrino telescoop zal astrofysische neutrinos zoeken op energieën waar icecube te klein voor is. Het zal ook het vinden van cosmogenische neutrinos mogelijk maken. Alle simulaties werden mogelijk gemaakt door de volgende programmas:

- NuRadioMC
- radiotools
- RadioPropa

Dewelke te downloaden zijn op github Deze master thesis is opgebouwd uit 3 delen. Hoofdstukken 2 t.e.m 4 zijn achtergrondinformatie, waarna in hoofdstuk 5 het bouwen van een algoritme uitgelegd wordt en in hoofdstuk 6 worden indirecte metingen gedaan gebruik makende van gemeten weerballon data. Het algoritme werd gebouwd in de eerste helft van het jaar en heet de *Hybrid minimizer*: een algoritme gemaakt met als doel het snel vinden van een pad vanuit een radio bron vertex (bv een neutrino interactie) tot de detector in complexe ijsmodellen. De indirecte metingen werden verwerkt in de tweede helft van het academiejaar, hier werd gebruik gemaakt van de locatie-info van de weerballon en de response van de detectors om een schatting te maken van de index van refractie lokaal aan de verscheidene channels van de detectoren. De code dienend tot het testen van het gemelde algoritme en het uitvoeren van genoemde simulaties kan hier gevonden worden en het algoritme zelf kan hier gevonden worden onder de branch radiopropa/hybrid_minimizer

CONTENTS

CHAPTER

1

NEUTRINOS

When looking outside into the night sky you might see various stars, but invisible to the naked eye various kinds of particles are also traversing light-years to end up where you stand.

When looking at phenomena outside our earth the astronomer will turn to electromagnetic radiation, as a lot of the most interesting events emit photons in some kind of way. But he's missing out on a big part of the full picture. There are regions in the universe from which photons can't escape. They can also be absorbed on their way to earth. That's where the astroparticle physicist comes in who takes a look at muons, nuclei,... and neutrinos.

Neutrinos are often called "ghost" particles because they very rarely interact with matter, on average 100 trillion neutrinos pass through your body per second, none of them having any effect. You'd even need a light year of lead to give you just a 50% chance of stopping a neutrino.

As they also have no charge they are not deflected by magnetic fields. This means that once a cosmic neutrino is detected and it's direction is inferred, it's origin can be found.

Because they can travel huge distances without getting distorted or sidetracked, neutrinos are ideal messengers to identify sources of ultra high energy (UHE) cosmic rays in the universe. Neutrinos can serve as unique clues about what's happening elsewhere in the universe including the cosmic collisions, galaxies, supernovae, Gamma-ray bursts (GRBs),... where they are created.

1.1 Discovery

When researching β^- decay, the decay of a neutron, researcher detected a proton and an electron coming from the neutron. However on closer inspection it became apparent that energy was lost somewhere in violation with the conservation law of energy, and angular momentum wasn't conserved. The solution postulated by Wolfgang Pauli was to introduce a new, really hard to detect particle with no charge and a very small mass: the neutrino. The neutrino comes in three flavours: electron, muon and tau neutrinos, each corresponding to their respective lepton

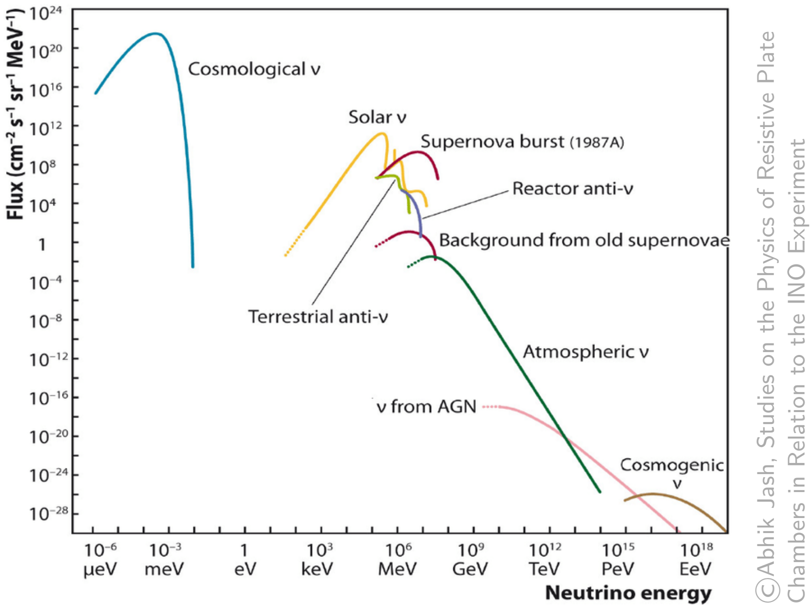

Figure 1.1: Predicted neutrino flux for various natural sources

denoted as

$$\nu_e \quad \nu_\mu \quad \nu_\tau \tag{1.1}$$

and each also having an anti-particle.

$$\bar{\nu}_e \quad \bar{\nu}_\mu \quad \bar{\nu}_\tau \tag{1.2}$$

Now with the introduction of the neutrino the full β^- decay becomes

$$n \rightarrow p^+ + e^- + \nu_e \tag{1.3}$$

The inverse can then also be used to detect neutrinos:

$$n \rightarrow p^+ + e^- + \nu_e \tag{1.4}$$

Which is called beta capture and was first experimentally detected in 1956 [5] also making it the first experimental detection of a neutrino.

1.2 Neutrino sources

Neutrinos can be generated in 2 ways: either they're generated in interactions at the sources, termed *astrophysical neutrinos*. Or they're created through the interaction of ultra-high energy cosmic rays during propagation with the cosmic microwave or other photon backgrounds termed *cosmogenic neutrinos*. In figure 1.1 you see the neutrino flux theoretically expected in function of energy for various sources of neutrinos. I'll walk you through each of them seperately, going from smallest energy and flux to highest.

1.2.1 Cosmological/Primordial neutrinos

The first source of neutrinos we'll talk about is the one in blue to the left of the figure termed the *Cosmological neutrinos*: the neutrino version of the CMB. To understand this source we'll have to go back all the way to just after the big bang: The very early universe was hot and dense.

As a result, interactions among particles occurred much more frequently than they do today. As an example, a photon today can travel across the observable universe without deflection or capture, so it has a mean free path greater than 10^{26} m. When the universe was 1 second old, though, the mean free path of a photon was about the size of an atom. Thus in the time it took the universe to expand by a factor of 2, a given photon interacted many, many times. These multiple interactions kept the consitituents in the universe in thermal equilibrium. But as the universe expanded there were times when reactions could not proceed rapidly enough to maintain equilibrium conditions, these particles then fall out of thermal equilibrium. This falling out of equilibrium is termed *decoupling*. And we're interested in when neutrinos decoupled. Neutrinos were kept in equilibrium through the interaction

$$\nu e \leftrightarrow \nu e \tag{1.5}$$

up until the universe cooled down to about 1MeV when they decoupled. To estimate the temperature of the neutrinos who decoupled at the start of the universe, we can take a look at conservation of entropy [6] from which we'll find that:

$$T_\nu = \left(\frac{4}{11}\right)^{1/3} T_\gamma \tag{1.6}$$

Note that they decoupled before the photons making them lower in temperature. As T_γ is the CMB temperature which, nowadays, is measured to be around 2.7K, these primordial neutrinos are very low in energy.

1.2.2 Solar neutrinos

The sun fuses elements to release energy and thus keeping itself from collapsing in on itself, with most of the various ways particles get fused, neutrinos get released:
pp – cycle

$$\mathrm{p} + \mathrm{p} \to \mathrm{D} + e^+ + \nu_e \tag{1.7}$$
$$\mathrm{D} + \mathrm{p} \to {}^3\mathrm{He} + \gamma \tag{1.8}$$
$${}^3\mathrm{He} + {}^3\mathrm{He} \to {}^4\mathrm{He} + \mathrm{p} + \mathrm{p} \tag{1.9}$$

boron – cycle

$${}^4\mathrm{He} + {}^3\mathrm{He} \to {}^7\mathrm{Be} + \gamma \tag{1.10}$$
$${}^7\mathrm{Be} + p \to {}^8\mathrm{B} + \gamma \tag{1.11}$$
$${}^8\mathrm{B} \to {}^8\mathrm{Be}^* + e^+ + \nu_e \tag{1.12}$$
$${}^8\mathrm{Be}^* \to {}^4\mathrm{He} + {}^4\mathrm{He} \tag{1.13}$$

Be – capture

$${}^7\mathrm{Be} + e^- \to {}^7\mathrm{Li} + \nu_e \tag{1.14}$$

pep

$$\mathrm{p} + e^- + \mathrm{p} \to \mathrm{D} + \nu_e \tag{1.15}$$

Now with this and some information about the sun like the pressure and mass, the so-called "standard solar model" was made. This model predicted a certain amount of neutrinos to be hitting the earth from the previously mentioned thermonuclear fusion, it was however 3 times higher than the observed amount of neutrinos back at our planet. This led to a little bit of hysteria as this could've meant that the sun was dying and we'd see the aftermath only in a couple of years. Through various experiments however, it became apparent that this was due to the different kinds of neutrinos oscillating into each other on their way to earth, i.e 2/3 of the original electron neutrinos had oscillated into mu and tau neutrinos. But for them to oscillate into eachother, they not only require mass but each flavor also should have a different mass as can be seen from an example 2D approximation to the transition probability:

$$P(\nu_e \to \nu_\mu) = |\langle \nu_\mu|\psi(L,T)\rangle|^2 = c_\mu c_\mu^* = \sin^2(2\theta)\sin^2\left(\frac{\Delta\phi_{12}}{2}\right) \tag{1.16}$$

with

$$\Delta\phi_{12} \approx \frac{m_1^2 - m_2^2}{2p} L \tag{1.17}$$

In full generality (3D):

$$|\nu_\alpha\rangle = \sum_i U_{\alpha i} |\nu_i\rangle \tag{1.18}$$

With $U_{\alpha i}$ the Pontecorvo-Maki-Nakagawa-Sakata (PMNS) matrix. This phenomenon has been observed e.g through the descrepency from the observed and expected neutrino events coming from a nuclear reactor [7].

1.2.3 Supernovae

A star starts its life as a ball of pure hydrogen. At the core, due to the gravitational pressure of the outside plasma, fusion of hydrogen into deuterium and helium happens. Thus converting mass into energy. The pressure of this energy counteracts the pressure of gravity and the star is stable.

When the hydrogen at the core runs out no more hydrogen can be fused. For stars with masses between $8M_\odot$ and $30M_\odot$ the fusion of heavier elements starts, this can't keep going on however as at some point the star starts to form the most stable element: iron. It costs energy to both

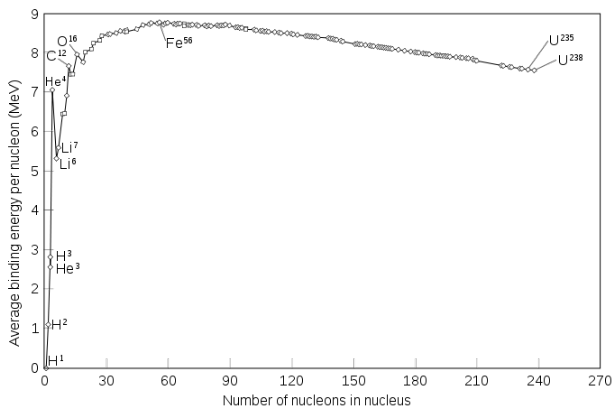

Figure 1.2: Energy per nucleon i.f.o number of nucleons in the nucleus

make lighter elements than iron and heavier ones. As the iron core builds up the outside pressure from the core starts to decrease as no new energy is released. This goes on until the treshold of an iron core with a mass of $1.4M_\odot$ known as the Chandrasekhar limit is reached and the the inwards pressure becomes too large, making the electrons surrounding the iron core fuse with

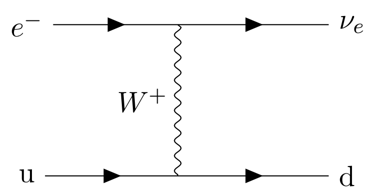

Figure 1.3: fusion of protons with surrounding electrons into neutrons via the weak force

the protons (uud), creating neutrons (udd) and neutrinos, diagramatically shown in figure 1.3. This last part happens in a split second as the collapse goes at 25% the speed of light, creating a very dense neutron star (3000km in diameter iron core to 30km in diameter neutron star) and up to 10^{52} ultra-relativistic neutrinos, carrying up to 99%[1] of the released energy [16]. As the density has suddenly increased so much there's a huge distance of pure vaccuum between the plasma outer layer and the (now) neutron star, this plasma starts free-falling inwards, also at 25% the speed of light whilst the neutrinos carrying tremendous amounts of energy start going outwards from the neutron stars core.

The neutrinos then collide with the plasma resulting in what we observe as a "supernova", wrongly thought of by Kepler as being a "new (nova) star" rather being a violent death of an old star.

This is quite unexpected as neutrinos rarely interact, it's only as the incoming plasma is so dense and due to the tremendous amount of neutrinos that collissions happen at all. Some, however, escape and will be visible on earth in our neutrino detectors $\approx$ 18h before the light escapes the exploding star.

Neutrino observatories are thus also useful to know where to point our various telescopes before the supernova is actually visible in the night sky.

1.2.4 Terrestrial anti-neutrinos

Terrestrial anti-neutrinos, also termed *geoneutrinos* are neutrinos coming from the decay of radionuclides (unstable nuclides due to excess in nuclear energy) naturally occuring in our earth. Most geoneutrinos are electron antineutrinos originating in β^- decay modes of ^{40}K, ^{232}Th and ^{238}U. Together these decay chains account for more than 99% of the present-day radiogenic heat generated inside the Earth

1.2.5 Reactor anti-neutrinos

Arguably our most important energy source today, both in terms of energy output and their impact on the enviroment are fission reactors. Looking back at figure 1.2 we see that all the way to the right uranium is found, a lot of energy can thus be released by splitting in into nuclei with a lower amount of nucleons. Fission reactors operate by splitting this urantium via the introduction of a neutron:

$$n + {}^{235}U \rightarrow \text{Energy (radiation)} + 2 \times \text{Fission fragments} + 2.5 \times n \tag{1.19}$$

this 2.5 is of course an average. The surplus of neutrons means that this is a self-sustaining reaction implying that for a stable thermonuclear fission reaction, carbon capture rods are needed. When this uranium nucleus fissions into two daughter nuclei fragments, about 0.1

[1] $\approx$1% is released as kinetic energy, only 0.001% as electromagnetic radiation

percent of the mass of the uranium nucleus appears as the fission energy which is about 200 MeV. For uranium-235 about 169 MeV appears as the kinetic energy of the daughter nuclei , the neutrons carry a mean kinetic energy per neutron of 2 MeV (total of 4.8 MeV) and 7 MeV is released in the form of gamma ray photons. This all sums up to the *total prompt fission energy* which amounts to about 181 MeV, or 89% of the total energy which is eventually released by fission over time. The remaining 11% is released in beta decays where we get our reactor anti-neutrinos from.

1.2.6 Background from old supernovae

Also termed the *diffuse supernova neutrino background* (DSNB), as the universe is quite old various supernovae have happened over it's lifetime, each generating a lot of neutrinos as was discussed in section 1.2.3. This is postulated to have generated a continuous neutrino background.

1.2.7 Cosmic rays

Before we can talk about atmospheric neutrinos it's necessary to discuss *cosmic rays*. Cosmic rays are ionized nuclei of which 90% are protons, 9% are alpha particles and the rest are heavier nuclei. Almost all of them originate from outside the solar system but from within our galaxy, the few particles that do come from our solar system can be temporally linked to violent events on the sun. In contrast to this the particles coming from outside our solar system show an anti-correlation with the sun as they can more easily reach the earth if solar activity is low. It has been observed that they roughly follow a power-law spectrum $N \propto E^{-\gamma}$ [8].

1.2.8 Atmospheric neutrinos

Cosmic rays hit the Earth's atmosphere at a rate of about 1000 per square meter per second and interact with atomic nuclei in the Earth's atmosphere, creating showers of particles, many of which are unstable and produce neutrinos when they decay, these neutrinos are what's called *Atmospheric neutrinos*. Most notably neutrinos can be produced together with muons in the two-body decays of charged pions and kaons wherever these hadronic interactions occur. The most important production channels and their branching ratios for neutrinos are:

$$\pi^{\pm} \rightarrow \mu^{\pm} + \nu_{\mu}(\bar{\nu}_{\mu})(\sim 100\%) \tag{1.20}$$

$$K^{\pm} \rightarrow \mu^{\pm} + \nu_{\mu}(\bar{\nu}_{\mu})(\sim 63.5\%) \tag{1.21}$$

Neutrinos are subsequently also produced when these muons decay:

$$\mu^{\pm} \rightarrow e^{\pm} + \nu_e(\bar{\nu}_e) + \bar{\nu}_{\mu}(\nu_{\mu}) \tag{1.22}$$

which is a process mainly happening at low energies in the atmosphere. The atmospheric neutrino spectrum shown in figure 1.1 roughly follows a power spectrum as the cosmic ray flux follows a power spectrum but the correspondence isn't one-to-one as, due to the difference in kinematics, the contribution from kaons to neutrinos is significantly more important than to muons, especially at high energies.

1.2.9 neutrinos from AGNs

An AGN (active galactic nucleus) is deemed to be the reason why several abnormal galaxies exist with an extra bright (and mostly variable) light source in their core which even the biggest of telescopes can't spatially discern. The general concensus is that this phenomenon is caused by one particular kind of object: a supermassive black hole (a black hole with a mass of at least $105\mathrm{M}_{\odot}$) surrounded with a close torus of dust and gas. This torus of gas is called an *accretion disc* and is an enormous source of energy. The conversion of potential energy of the incoming gas to highly energetic radiation is a very complex physical process with which we have to account for various factors like gravitational instabilities, magnetic fields, hydrodynamical turbulence,... And thus produces a spectrum that's quite complex. It would appear that the luminocity of an AGN would increase indefinitely with incoming mass, but this process is limited: if too much matter accretes on the black hole the radiative pressure becomes too massive and the matter on the disc gets blown away, this phenomenon is termed a *black hole outburst*.

The emission of high energy neutrinos from AGNs rests solely on the premise that relativistic protons of sufficiently high energy and energy density in the AGN's accretion disc will be present [15] as they may interact to create e.g pions whom decay. A direct consequence of the occurence of these relativistic protons is the production of γ-rays of similar energies to those of the neutrinos, thus high energy neutrino- and γ-ray astronomy are closely related. However, even though γ-ray photons can be produced even in the absence of relativistic protons (e.g via high energy electrons), neutrinos can not. Thus the detection of these high-energy neutrinos (which might have already been detected [4]) will provide unique information about the workings of AGNs.

1.2.10 Cosmogenic neutrinos

And now finally one of the most exciting neutrino sources (maybe) observable on earth: cosmogenic neutrinos. The mechanism by which these get created is quite simple, if a proton has sufficiently high energy the cross section to interact with CMB (Cosmic Microwave Background) photons becomes non-negligable. These protons can scatter off the photons to resonantly produce a Δ^+ baryon. This resonance has enough mass to dominantly decay to a pion and a nucleon:

$$\Delta^+ \to \pi^0 + p \quad (2/3) \tag{1.23}$$
$$\Delta^+ \to \pi^+ + n \ (1/3) \tag{1.24}$$

Of which the charged pion decays to neutrinos as previously mentioned in 1.2.8.

1.2.11 How do they fit into the full detector spectrum?

The origin of the most energetic cosmic rays is still not conclusively identified. One approach to solving this problem is *multi-messenger astrophysics*, where several types of cosmic particles are used to identify the sources of these ultra-high energy cosmic rays (UHECRs). E.g we simultaneously measure gravitational waves with the Einstein telescope, neutrinos with IceCube (or eventually RNO-G), photons with various telescopes and muons with a muon detector.

1.3 Current research

There are still a lot of unknowns concerning neutrinos, for the interested reader here I'll quickly go over current research into the most prominent questions. Namely "How do neutrinos get their mass? (theoretically)" and "are neutrinos Majorana?".

1.3.1 Mass

As neutrinos oscillate they must have mass, the currently most exciting theory to explain the origins of this mass is the *See-Saw mechanism* here mass is given via a simple Yukawa coupling:

$$\mathcal{L} = i\bar{\nu}\partial\!\!\!/\nu - m\bar{\psi}\nu - \frac{M}{2}(\bar{\nu}_R\nu_{Rc} + \bar{\nu}_{Rc}\nu_R) \tag{1.25}$$

The exciting part about this theory however is that you can re-write this with

$$\chi := \frac{1}{\sqrt{2}}(\psi_R + \psi_{Rc}) \tag{1.26}$$

$$\omega := \frac{1}{\sqrt{2}}(\psi_L + \psi_{Lc}) \tag{1.27}$$

And after some math find that you'll get the eigenvectors $\phi_\pm$ with eigenvalues $m_\pm$:

$$\phi_\pm := \begin{pmatrix} x_\pm \\ y_\pm \end{pmatrix} = \begin{pmatrix} \frac{\lambda_\pm}{\sqrt{\lambda_\pm^2+m^2}} \\ \frac{m}{\sqrt{\lambda_\pm^2+m^2}} \end{pmatrix} \quad \text{and} \quad m_\pm := \lambda_\pm = \frac{M}{2}\left(1 \pm \sqrt{1+4m^2/M^2}\right) \tag{1.28}$$

Now in the limit $M \gg m$, in the χ, ω basis:

$$m_+ \approx M \quad \text{with eigenstate} \quad \chi + \frac{m}{M}\omega \tag{1.29}$$

$$m_- \approx -\frac{m^2}{M} \quad \text{with eigenstate} \quad \omega - \frac{m}{M}\chi \tag{1.30}$$

$$\tag{1.31}$$

This is why it's called the See-Saw mechanism : For a certain m if we choose a big M we'll get a big m_+ and small m_- (and vice versa). We also see that there's only a very small mixing of states, i.e the m_- mass state is almost purely ω (and m_+ almost purely χ). The parameter m in the original matrix is forbidden by electroweak gauge symmetry, and can only appear after the symmetry has been spontaneous broken by a Higgs mechanism; for this reason a good estimate of the order of m is the vaccuum expectation energy: $m \approx v = 246 \approx 10^2$GeV. In grand unified theories it's theorised that $M \approx 10^{15}$GeV after symmetry breaking, using these values we get

$$m_- \approx 10^{-11}\text{GeV} \approx 10^{-2}\text{eV} \tag{1.32}$$

which seems [2] to be a reasonable order of magnitude estimate for the observed neutrino mass. This mechanism would also lead to supermassive neutrinos, which are a possible dark matter candidate.

1.3.2 Majorana

A theory that's also quite interesting is that neutrinos are majorana, meaning that they are their own anti-particle. A dirac fermion has the following density:

$$\mathcal{L} = i\bar{\psi}\not{\partial}\psi - m\bar{\psi}\psi \tag{1.33}$$

$$= i\bar{\psi}_L\not{\partial}\psi_L + i\bar{\psi}_R\not{\partial}\psi_R - m\bar{\psi}_R\psi_L - m\bar{\psi}_L\psi_R \tag{1.34}$$

Now assume that we only have right-handed particles:

$$\mathcal{L} = i\bar{\psi}_R\not{\partial}\psi_R - \frac{M}{2}\bar{\psi}_R\psi_{Rc} - \frac{M}{2}\bar{\psi}_{Rc}\psi_R \tag{1.35}$$

A majorana fermion is a fermion which is it's own anti-particle, i.e:

$$\chi = \frac{1}{\sqrt{2}}\left(\psi_R + \psi_{Rc}\right) = \chi_c \tag{1.36}$$

With this we can re-write equation 1.35 as:

$$\mathcal{L} = i\bar{\chi}\not{\partial}\chi - M\bar{\chi}\chi \tag{1.37}$$

Thus arriving at a density for Majorana fermions with mass M, this would be an exciting property for neutrinos as it would lead to the possibility of *Neutrinoless double beta decay*:

Figure 1.4: normal and neutrinoless double beta decay

CHAPTER

2

RADIO DETECTION OF NEUTRINOS

2.1 Neutrino interactions in ice

As neutrinos propagate through ice they can interact with nuclei in the following ways [9]:

Figure 2.1: Most prominent ways of neutrino-nucleus interaction

With the produced leptons in the W boson mediated interaction being either electrons, resulting in an electromagnetic shower, muons wich typically go undetected as they live too long or tauons wich will decay via

$$\tau^- \rightarrow e^- + \bar{\nu}_e + \nu_\tau \tag{2.1}$$

or, less ideally

$$\tau^- \rightarrow \mu^- + \bar{\nu}_\mu + \nu_\tau \tag{2.2}$$

In both of the possible interactions (W or Z exchange) the resulting nucleus will result in a hadronic shower, for the neutral current interaction (mediated by the Z boson) the fraction of the neutrino energy that gets transferred to the nucleon is described by the inelasticity y and is heavily shifted towards small values of y [1]. This causes a big, irreducable uncertainty when trying to estimate the original neutrino energy from these kinds of events. With the charged current interaction (mediated by the $W^{\pm}$ bosons) this isn't a problem however as the full neutrino energy ends up in the resulting cascades.

2.2 Askaryan effect

For a particle shower to emit strong radio signals, two conditions have to be met:

- There needs to be a separation of positive and negative charges in the shower front
- The signals produced over the length of the shower profile need to overlap coherently.

The *Askaryan* [3] effect, also known as Askaryan radiation describes the effect at radio frequencies which abides by both of these conditions, in general it's a quite difficult effect but we'll give a crude overview. The previously described interactions create a shower of secondary charged particles containing a charge anisotropy, this charge imbalance is a result of medium electrons either Compton scattering into the advancing shower or annihilating with shower positrons. In the end you have a moving charge anisotropy, propagating faster than the speed of light in the medium, creating Cherenkov radiation. Cherenkov radiation is like the electromagnetic equivalent of a sonic boom, a sonic boom happens when something goes faster than the speed of sound in the medium; A particle emits Cherenkov radiation if it goes faster than the speed of light in the medium[1] . Choosing the particle trajectory to lie along the z axis we can approximately find an equation for $\frac{\mathrm{d}^2\mathscr{I}}{\mathrm{d}\omega\mathrm{d}\Omega}$: the energy radiated per elementary unit solid angle and per elementary unit frequency interval

$$\frac{\mathrm{d}^2\mathscr{I}(\omega)}{\mathrm{d}\omega\mathrm{d}\Omega} = \frac{q^2}{4\pi}\sqrt{\frac{\mu}{\epsilon}}\beta^2\omega^2\delta^2[\omega(1-\beta\mathbf{e}_r\cdot\mathbf{e}_z)]|\mathbf{e}_r\times\mathbf{e}_z|^2 \tag{2.3}$$

Now we can re-write this equation in spherical coordinates, which gives $1-\beta\mathbf{e}_r\cdot\mathbf{e}_z = 1-\beta\cos(\theta_c)$ in the delta function. We thus only expect radiation if

$$\cos(\theta_c) = \frac{1}{\beta} = \frac{c'}{u} = \frac{c}{n}\cdot\frac{1}{u} \tag{2.4}$$

I.e if $u > \frac{c}{n}$ with n the index of refraction, Cherenkov radiation will be emitted along a cone surface with half angle $\frac{\pi}{2}-\theta_c$ as illustrated in figure 2.3. Integrating equation 2.3 over the solid angle and formally dividing by the time interval we get:

$$\frac{\mathrm{d}^2\mathscr{I}}{\mathrm{d}\omega\mathrm{d}t} = \frac{q^2}{4\pi}\sqrt{\frac{\mu}{\epsilon}}\beta\omega\left(1-\frac{1}{\beta^2}\right) \tag{2.5}$$

We see that the energy is proportional to ω, so we expect that most radiation will be emitted "in blue", as seen in figure 2.2. For ice the index of refraction is roughly 1.78 in deep ice, so we expect an ultra-relativistic particle to produce the most radiation at around 56° opening as

$$\cos(\theta_c) \approx \frac{1}{n} \implies \cos^{-1}\left(\frac{1}{1.78}\right) \approx 56^\circ \tag{2.6}$$

Of course this is just an estimate, as the actual index of refraction is depth-dependent which we'll get to in section 2.5. Now this explains how the signals get generated but logically, from only knowing this we'd expect radio waves to almost be non-existent due to the "in blue" nature of Cherenkov radiation. This isn't the full story however as we'll need to talk about coherent overlap to fully understand the Askaryan effect. This can be intuitively explained as follows: generally the shower is of length $\mathcal{O}(10\text{cm})$ [14], over this length the radiation gets emitted, most frequencies decoherently interfering, but radio waves with wavelengths of ≈ 10cm coherently interfere, and it's these waves we then wish to detect.

[1] The reader who wants a thorough explanation and derivation is advised to check out *Chapter 14: Radiation by Moving Charges* from the book *Classical Electrodynamics* by Jackson.

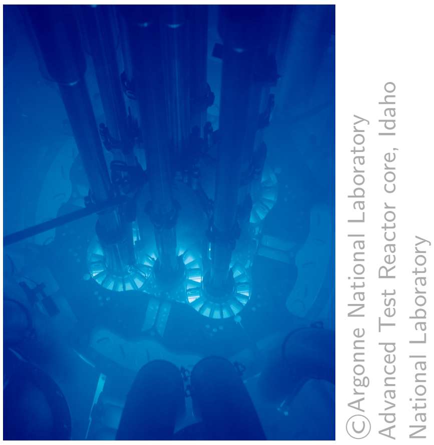

Figure 2.2: Cherenkov radiation in a nuclear reactor

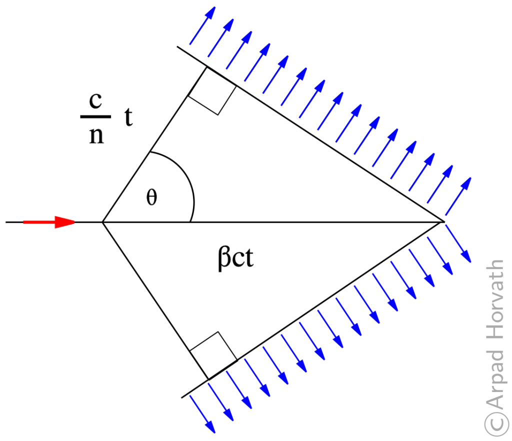

Figure 2.3: Diagrammatic representation of Cherenkov radiation

2.3 Polarization

The generated electromagnetic radiation is polarized perpendicular to the cherenkov cone, this can be useful to discern between two cherenkov cones whom, timely, would generate the same response. This concept is illustrated below where two neutrinos from different directions would generate the same signal in the detector. If the detector has a way to differentiate between polarization however, there would be no doubt where the neutrino originated from as the one producing the yellow cherenkov cone would have a downwards polarization and the one producing a green cherenkov cone would have an upwards polarization.

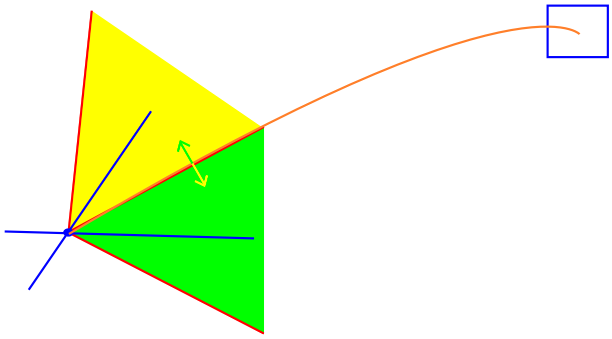

2.4 Wave propagation

Waves propagating through ice to detectors generally looks something like what's illustrated in figure 2.4. Here the interaction of the neutrino happens somewhere in the neighbourhood of the red cross, the orange rays represent the resulting radio wave paths to the detector channels which are illustrated by blue dots. Notice that reflection at the surface is also a possible path to the detector. In a dielectric medium a ray propagates with it's signal wave-speed determined by the local index of refraction as $v = c/n$. The dependence of the index of refraction on density for ice is given by the Schytt equation:

$$n(x, y, z) \approx 1 + 0.78\rho(x, y, z)/\rho_0 \tag{2.7}$$

Where $\rho(x, y, z)$ is the local ice density and ρ_0 is the density for solid ice (917 kg/m^3). The effect on speed isn't the only effect the index of refraction has which we'll need to concern ourselves

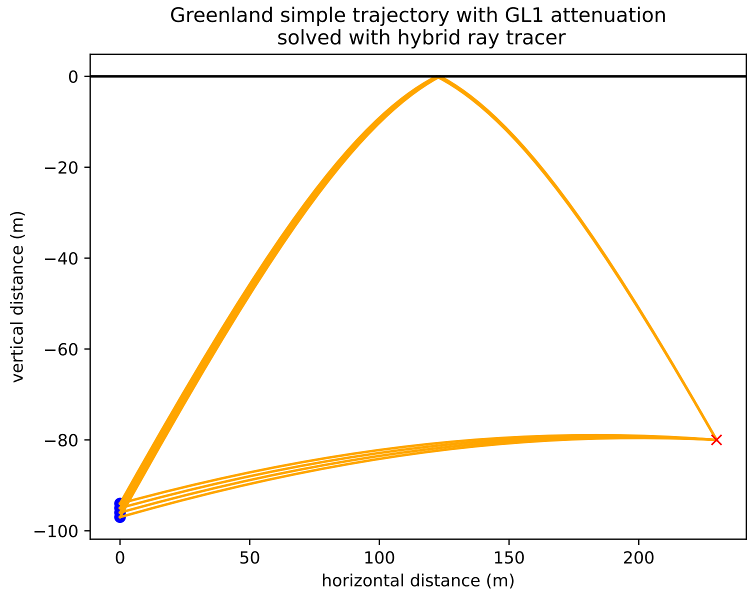

Figure 2.4: illustration of radiowave paths generated by a neutrino event

with however, if a ray propagates towards a boundary dividing 2 media with different indexes of refraction, the ray will refract and the refracted angle can be found from Snell's law:

$$n_1 \sin\theta_1 = n_2 \sin\theta_2 \tag{2.8}$$

Where n is the index of refraction and θ is the angle with respect to the surface normal. The system we'll consider however, isn't homogeneous with some specified boundary, it's continous: ice in greenland has a continously varying density. Because of this we can't work with Snell's law but we'll have to take a look at the continuous version to figure out how these rays propagate. The "continuous version of Snell's law" is the eikonal equation: a path of a ray $\mathbf{r}(s)$ with path parameter s in a medium with index of refraction n($\mathbf{r}$) is described by:

$$\frac{d}{ds}\left(n(\mathbf{r})\frac{d\mathbf{r}}{ds}\right) = \nabla n \tag{2.9}$$

The software we'll be using for ray reconstruction is called "radiopropa" [20] and in radiopropa the local paraxial approximation is used, i.e. if we assume that in any individual step of the algorithm the change of the refractive index along the path ds is small it's possible to re-write the equation as:

$$n(\mathbf{r})\frac{d^2\mathbf{r}}{ds^2} \approx \nabla n \tag{2.10}$$

Which is then easily iteratively solved. If there are boundaries (such as defects or the surface) these are treated seperately using Snell's law.

2.5 Ice model

Equation 2.10, and thus the path, depends on the index of refraction on a given location. Purely from classical gravity and density considerations it can be derived that the index of refraction abides by

$$n(z) = n_{ice} - \Delta n e^{z/z_0} \tag{2.11}$$

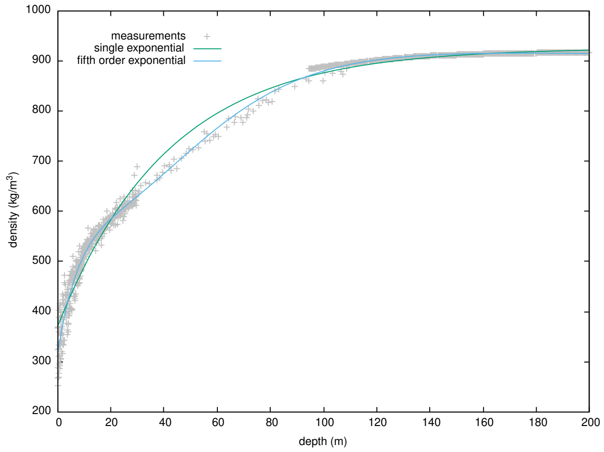

Figure 2.5: Measurements of the density (kg/m^3) i.f.o the depth with various fits

with n_{ice} the refractive index of solid ice and $\Delta n = n_{ice} - n_s$ with n_s the index of refraction of snow. This is called "the exponential model". Looking back at Schytt's equation we see that this model is a consequence of the exponential nature the density would have.

This exponential model has a huge advantage as it's analytically solvable, meaning that we don't have to iteratively search for the path to the detector but know it instantly after the location of the neutrino interaction and the detector are specified, the ray tracing software developed in complience with this exponential density profile is called the *analytic ray tracer*.

There is one big downside however: looking at measurements of the density i.f.o depth as shown in figure 2.5 And fitting the "exponential model" which can be derived by combining equations 2.7 and 2.11 to the form

$$\rho_0(n_{ice} - 1 + \Delta n e^{z/z_0}) = \rho \tag{2.12}$$

or simply

$$a(b + ce^{z/d}) = \rho \tag{2.13}$$

it seems that the ice actually doesn't follow this exponential curve perfectly but more closely some kind of polynomial. as an example the curve "fifth order exponential"[2] was included which has the structure

$$a_5 exp(-z/z_0)^5 + a_4 exp(-z/z_0)^4 + a_3 exp(-z/z_0)^3 + a_2 exp(-z/z_0)^2 + a_1 exp(-z/z_0) + a_0 \tag{2.14}$$

this discrepency between the exponential model and the actual data implies that the analytic ray tracer will make the wrong predictions. This is why the development of a different ray tracer was needed which will be able to handle more complex (e.g polynomial) ice models, we'll get to this ray tracer in chapter 4.

[2]This is just an example, a better function can probably be found

CHAPTER

3

THE DETECTOR

Both cosmic ray and neutrino detectors face the same main problem at the highest energies: the steeply falling flux (as was previously discussed in chapter 2) requires large effective areas, which leads to the construction of neutrino detectors with volumes on the cubic kilometer scale: IceCube. But even IceCube has it's limitations, it's still too small to observe neutrino events above the PeV scale, that's why a new detector was needed which was even bigger. We could just make IceCube bigger but this would cost a lot of money as the individual detectors need to be spaced closely as IceCube works in the visible spectrum for which the attenuation length is quite short. The proposed solution was to work with radiowave detectors, leveraging the Askaryan effect which has been previously explored e.g in the NuMoon project. Besides the advantage radiowaves have due to their abundance, they can also propagate way further in ice than visible light making it possible to space the individual detectors further apart. The proposed location was Greenland, an island country in North America and part of the Kingdom of Denmark which has large ice sheets. An orthographic projection projection of greenland is shown in figure 3.2 and both Greenland's flag and it's code of arms are shown in figure 3.1, the flag sports the same colors as it's parent country's flag Denmark. The flag is designed by Thue Christiansen who described the white stripe as representing the glaciers and ice cap, which cover more than 80% of the island; the red stripe, the ocean; the red semicircle, the sun, with its bottom part sunk in the ocean; and the white semicircle, the icebergs and pack ice. The design is also reminiscent of the setting Sun half-submerged below the horizon and reflected on the sea.

Figure 3.1: Flag (left) and Coat of arms (right) of Greenland

Figure 3.2: orthographic projection of Greenland

The proposal for RNO-G, which was later funded and now in the construction phase, is it be an array of autonomous radio stations each of which having both surface channels and various deep channels resulting in a total of 24 channels per station. The whole project builds heavily on the knowledge obtained through previous neutrino detectors like ARA, RICE and ARIANNA experiments, as well as the balloon-borne ANITA experiment.

One such detector is illustrated in figure 3.3, the plan is to build 35 of these as is shown in figure 3.4[1]. Looking closely at one such detector we see just below the surface 9 Log Periodic Dipole Antennas (LPDAs), these are used to detect muon signals as muons will also generate cherencov radiation in the ice whose signals can then be filtered out. Aside form these surface detectors there are also deep components of the detector which can be split up in three parts: Two *helper strings* and the *power string*.

The helper strings are the 2 vertical cables shown on the right of figure 3.3 each housing 2 vertically polarized antennas (Vpols), one quadslot antenna for the horizontal polarization component (Hpol) and one radio pulser on each helper string which can be used to generate calibration signals. As was mentioned in the previous chapter the polarization can be used to distinguish between 2 possible cherenkov cones generating the same resulting pulse, this effect will mostly concern vertical polarization, as such most of the deep channels are vpol antennae.

The power string (the leftmost vertical cable) is more densely instrumented than the helper strings: At the bottom it houses a set of four Vpol and two Hpol antennas with a spacing of 1m and further up the string, with a spacing of 20m, are three more Vpol antennas.

The signal from each of these antennae are fed into a low-noise amplifier directly above it, from there the signal is send to the data acquisition (DAQ) system at the surface via a Radio Frequency over Fiber (RFoF) cable. There it's again amplified, digitized and saved onto an SD card. This data is then transmitted via a Long Term Evolution (LTE) telecommunications network to a local server[2], from where it is sent via a sattelite link.

[1] note that all the individual detectors are named after various species living in greenland (in the native tongue)

[2] There is additionally a Long Range Wide Area Network (LoRaWAN) antenna as backup in case of problems with the LTE network

There are solar panels as a power source who charge up battery banks, but as there is't enough light during the Greenland winters, there're plans to build wind turbines (with one of the problems being the possibly detectable RF noise the 'engine' would produce).

It can,however, pose a challenge to reconstruct the radio signals produced by the Cherenkov radiation as they are often obscured by background noise. A solution used in RadioReco is Information Field Theory (IFT) implemented in RadioReco by Welling et al. [18] which uses Bayesian inference to calculate the most likely radio signal, given recorded data.

As was previously explained the radio signal from a neutrino often travels along both direct and refracted paths (designated DnR) to the deep array. This double pulse characteristic would be a smoking-gun signature of an in-ice source. The two helper strings are needed for a full direction reconstruction. Three independent measurements are needed for azimuthal information, which is provided by the Vpol (Vertical polarization) antennas and placing the Hpol (Horizontal polarization) antennas at different depths on every string, both zentih and azimuth information will be provided for those signals. The helper strings' calibration pulsers, as well as one on the surface, will ensure regular monitoring of the performance of the station and provide information useful for precise calibration of the antenna geometry.

Christoph Welling did an investigation into energy reconstruction from the received signals [19] for air showers in one single station (as the RNO-G stations are so far apart this is the case here aswell) and he noticed that it is nescessary to know if the detector who observes an event falls inside or outside the Cherenkov cone to accurately reconstruct the primary particle energy as most over-estimated energies in his simulations are caused by events viewed from within the Cherenkov ring being mistaken for events outside of it. He went on to show that, if we somehow know if the shower was seen from inside or outside the ring from some extra source, that most outliers in the energy disappeared. It is shown by Hiller et al. [13] that the combination of a muon detector with the radio detector might make the issue of confusion between being within or outside of the Cherenkov-ring disappear. Because of this the RNO-G stations are fitted with surface Log Periodic Dipole Antennas (LPDA), capable of detecting muons. Note that this is for air showers, the radio signal from neutrinos show additional complexities.

3.1 Reconstruction: Lookup tables

The main simulation code we'll be using consists of 2 parts: NuRadioMC [10] and NuRadioReco [11]. NuRadioMC uses Monte Carlo simulations to generate neutrino events in the ice and how they propagate to the various channels. NuRadioReco is reconstruction software, it simulates how the various detectors would respond to the detected radiowaves. The plan is to simulate a lot of neutrino events and record the detector responses in a giant database then, when an actual neutrino event occurs, we'll only have to look in the database and match the actual detector response to the simulated detector responses, thus finding the origin.

3.2 Reconstruction: Butterworth filters

Sometimes it is necessary to only let through a certain part of the frequency spectrum that's recorded, an elegant way to accomplish this is by using a Butterworth filter. This is a filter that's applied afterwards on the measurements and only let's through a certain part of the observed frequency spectrum

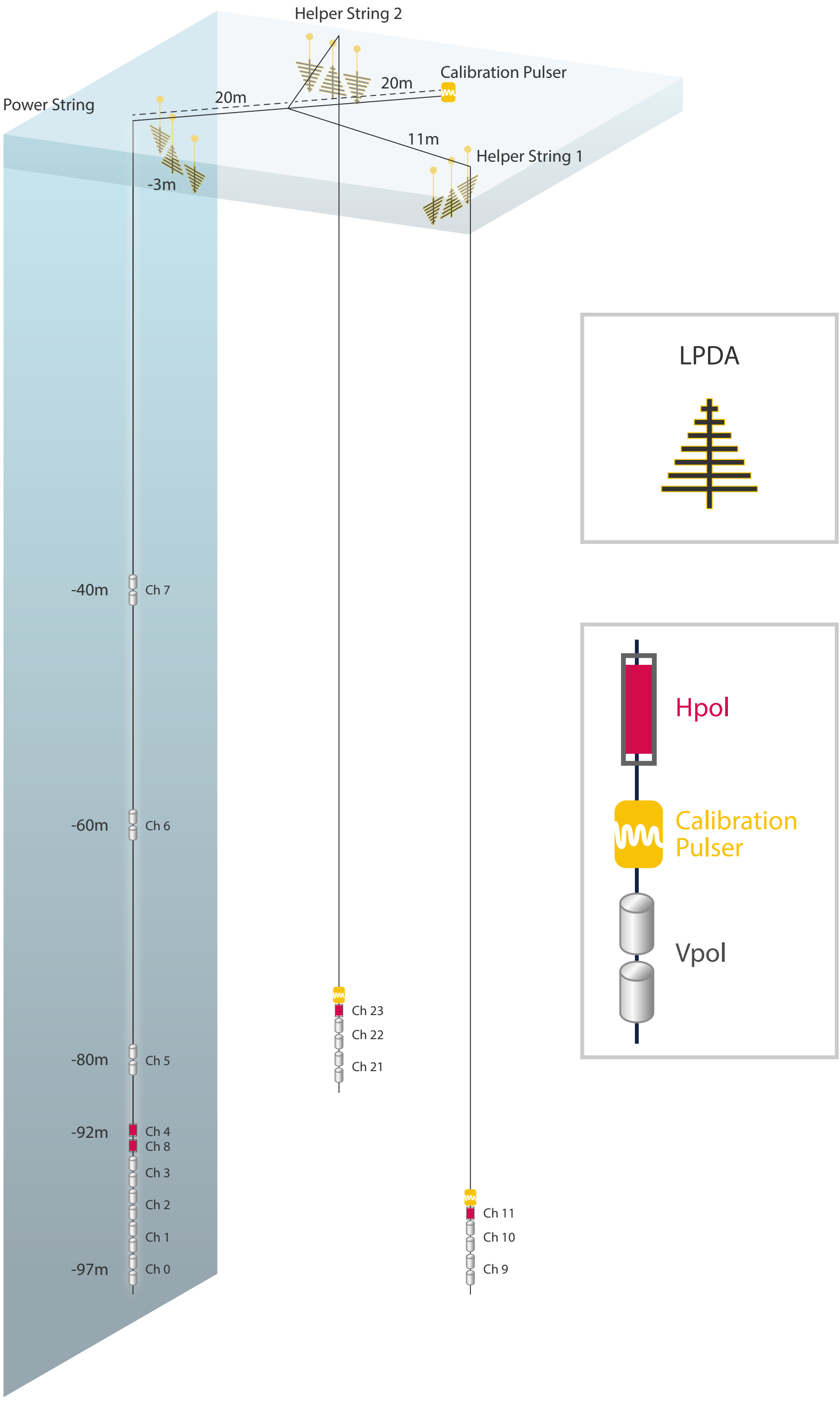

Figure 3.3: illustration of the detector

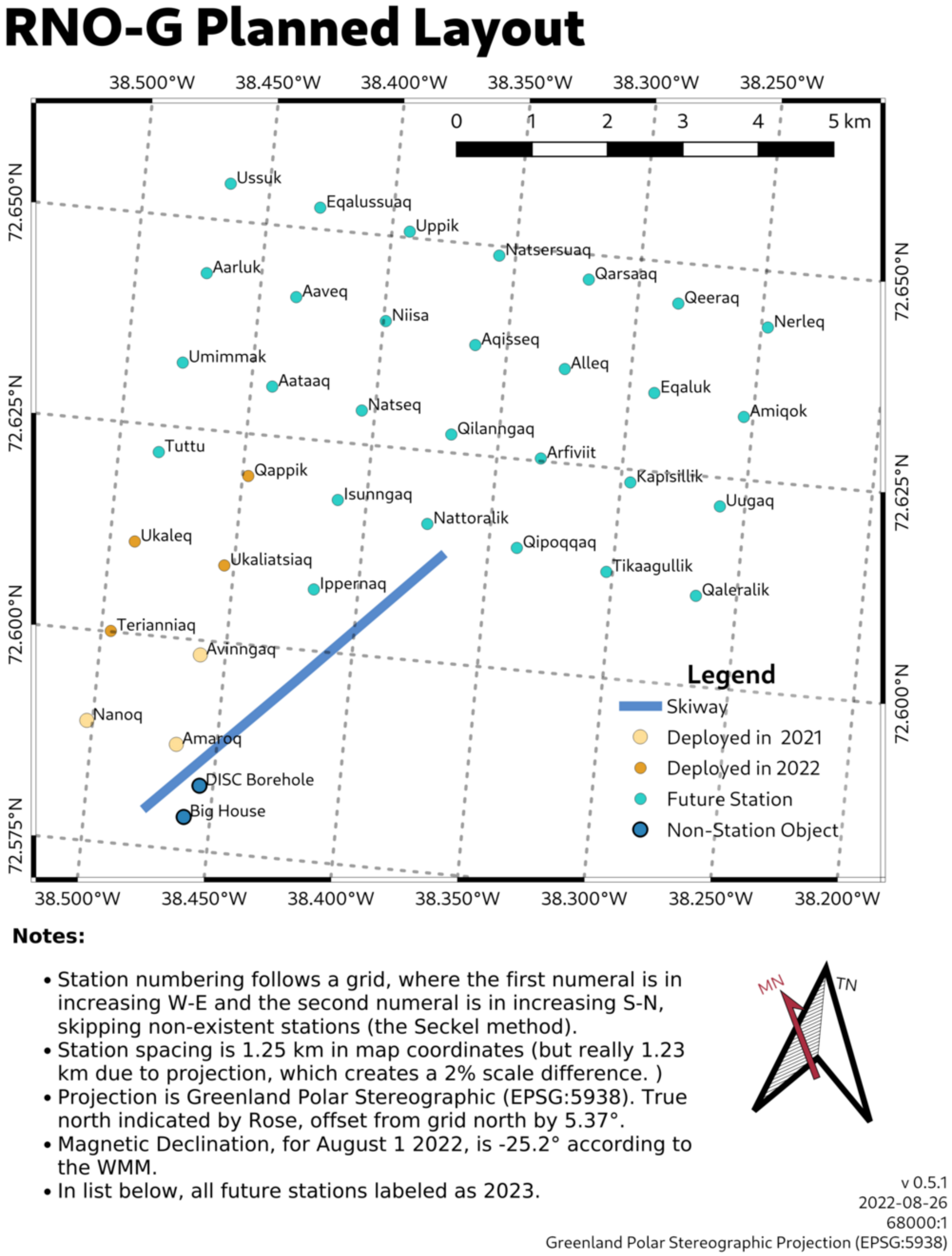

Figure 3.4: map of the station

CHAPTER

4

HYBRID RAY TRACER

4.1 Shortcomings of the exponential ice model

As mentioned in section 2.5, complex ice models will be necessary moving forward as the exponential ice model fails to fit the density curve. The ideal software for radio wave propagation through ice is radiopropa [20], but due to the way it works you'll have to know the start point, the end point and the launch angle of your ray to work out the path. This isn't difficult for the analytic model as it's exactly solvable but for a general ice model you'll somehow have to find where to *shoot* the ray. Work has been done on finding the launch angle in the case of complex ice models by B. Oeyen et al. [17], where they created a ray tracer which iteratively finds the solution, called the "iterative ray tracer". The full explanation of how their algorithm works can be found in the mentioned paper. This is however a sub-optimal solution in python as an optimalisation library will generally work faster, work had been done on trying to implement such an algorithm deemed the "minimizer" but this attempt failed. As we saw this work the idea came to mind to combine the iterative ray tracer and the code using the optimization libraries, to come up with the algorithm that will be discussed in this chapter: The hybrid ray tracer, in the source code called the "hybrid minimizer" which can be found here under the radiopropa/hybrid_minimizer branch.

It succeeds in more rapidly tracing the path from the event to the detector, is more accurate and also arrives closer to the detector as the final result is not limited by the final drawn sphere size but by a given tolerence making it useful for plane wave reconstruction as we'll get to next chapter.

4.2 How it works

The hybrid minimizer can be seen as an extension of the iterative raytracer [17] as it starts out the same way: Say our source of radiation is at position $\mathbf{X}_1$ and our detector is located at position $\mathbf{X}_2$, we start by defining the vector $\mathbf{v} = \mathbf{X}_2 - \mathbf{X}_1$, then we clone it as a new vector u and set u's z coordinate to 0, making it a normal vector of a plane parallel to the z direction. we now wish to know where we'd actually be able to find possible paths, looking at figure 2.4

we see that no solutions below the direct path are possible as there would need to be upwards reflection, so we convert our vector **v** representing the path from the source to the detector to spherical coordinates, giving us a polar angle (zenith angle) "theta-direct". With this we know that at the source the ray should propagate with an initial zenith angle within the angle interval 0° to theta-direct° := Ω.

Next we need to define our "observers", if you shoot a ray with the radiopropa module from a certain point at a certain angle the ray path will get simulated until it interacts with this "observer". Ideally we would like to a priori know where to shoot our ray and have the detector be an infinitesimally small observer in our simulation, but as we'll be working with general ice models this can't be done.

The algorithm of finding the possible paths is then as follows: We define a spherical observer at the location of the detector, with a radius of fair size. We place an observer plane directly behind the detector (with normal vector **u**, no rays can propagate back after crossing) and an observer above the surface (as no rays could make it back after escaping the ice) our full setup is then what's illustrated in the figure below

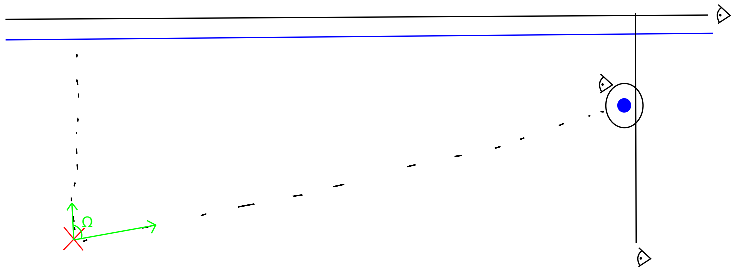

Here the red cross is the radio source, the blue horizontal line is the ice-air boundary surface, the blue dot to the right is the detector and the green Ω indicates the range over which solutions to the problem are possible.

We start off by just iteratively guessing: given a certain angle stepsize $\Delta\theta$ shoot rays at the angles $\{0, \Delta\theta, 2\Delta\theta, ..., \Omega\}$ And see which ones get detected at the sphere around the detector, this process is illustrated in a modified version of B. Oeyen et al. their figure below

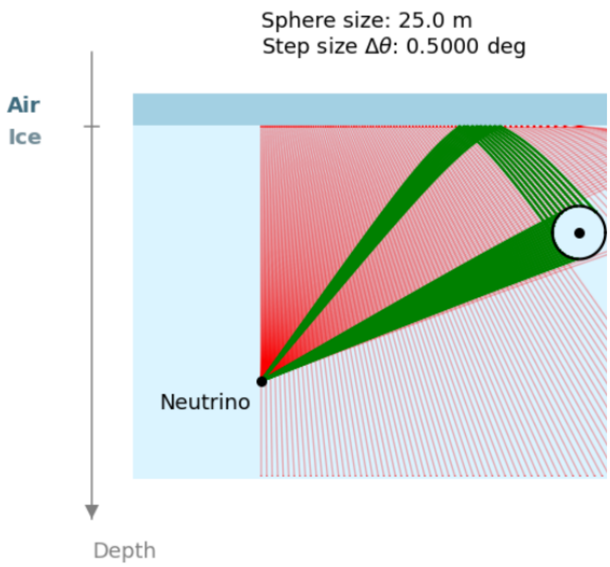

if there are 2 distinct launch regions, it will start the so called "minimization", using scipy's module optimize.minimize. First we get rid of the spherical observer and place the vertical observer exactly at the detector, now to be able to use the minimize module we'll need a function to minimze, for this reason we define the function *delta_z* as, given a certain launch angle, returning the distance from the point where it lands on the plane to the detector as illustrated below

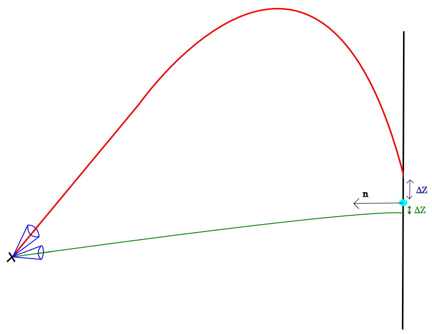

The function we'll minimize is then detla_z_squared which is just the square of delta_z as we wish it to be as close as possible to 0, it gets minimized within the angle boundaries found from the previous step. With this our algorithm is done, it does have a fail-safe as well for if the first step, finding the launch regions, doesn't work namely it reverts back to being the iterative ray tracer.

4.3 Performance Optimalisation

To test the hybrid minimizer the numpy random module was used to generate random coördinates, the considered square (as there is only a z component to the ice model the 3D problem is cilindrically symmetric and thus essentially only a 2D problem) is x:0.1km,4km and z:-0.1km,-3km.[1] Every test point shown in the following subsections consists of at least 500 random initial positions. As the speed of the algorithm is computer dependent the algorithm's speed is always plotted relative to the iterative ray tracer's speed, simulated with the same coordinates at the same time.

4.3.1 Length of the normal vector

As visually explained in figure 4.1, the size of the normal vector seems to influence how big the ray tracer's step size is taken close to the detector. This thus influences the convergence and time taken. The results of varying this are shown in figures 4.4 and 4.5. Looking at these figures the first optimization conclusion is as expected: take the normal vector length to be 1 meter.

4.3.2 ztol

We'll now change the tolerence on the vertical distance away from the detector which is deemed accepted i.e in figure 4.1 if Δz is below this threshold it's accepted. The results are shown in figures 4.6 and 4.7. From which we can conclude the second optimization conclusion: take ztol to be 0.05 m.

[1] This start at 100m depth was to get around issues concerning events that won't even trigger in a full simulation

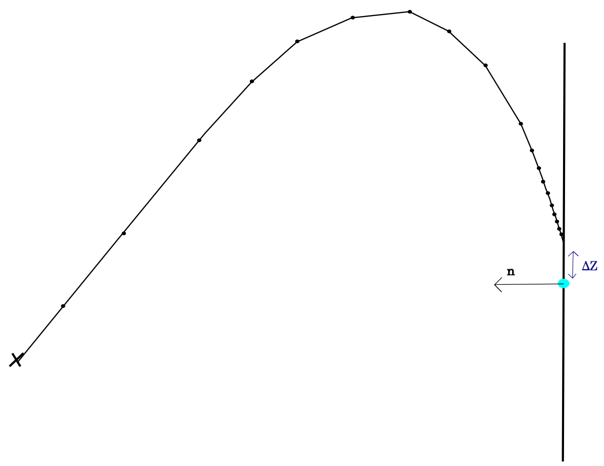

Figure 4.1: how normal vector size influences the stepsize

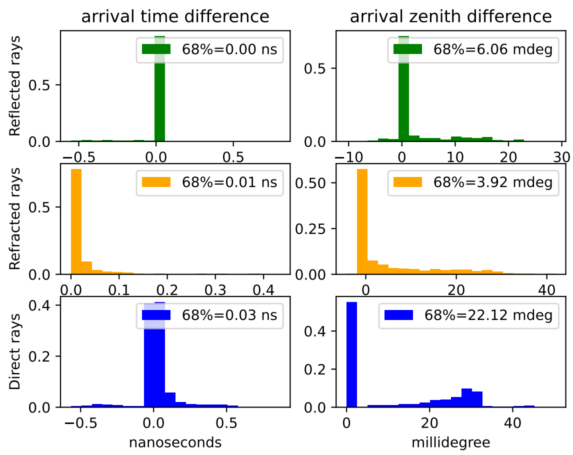

Figure 4.2: Hybrid

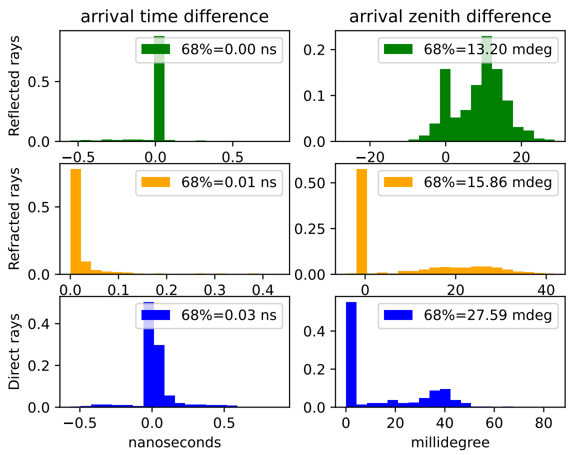

Figure 4.3: Iterative

4.3.3 Sphere Size & Step Size

The initial rays are sent out in steps of a certain angle and with a sphere around the detector of a certain size. As this initial search for launch angle regions is the slowest step in the hybrid ray tracer it's imperative to optimize this. The procedure was: change the sphere size and loop over various step sizes, recording the speed. The results are shown in figure 4.8 the lower on the chart the better, zooming in onto the lowest point as is shown in a combined plot on figure 4.9, we see that an optimum seems to be around a spheresize of 45m and a stepsize of 0.7°.

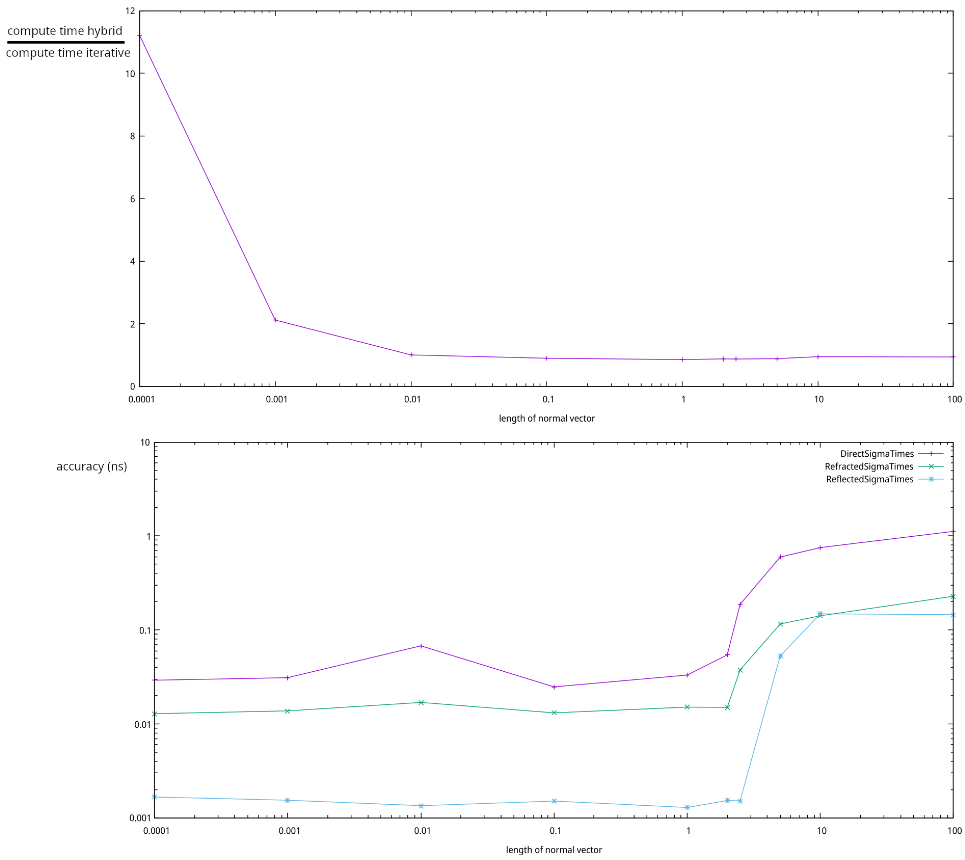

Figure 4.4: influence of the length of the normal vector

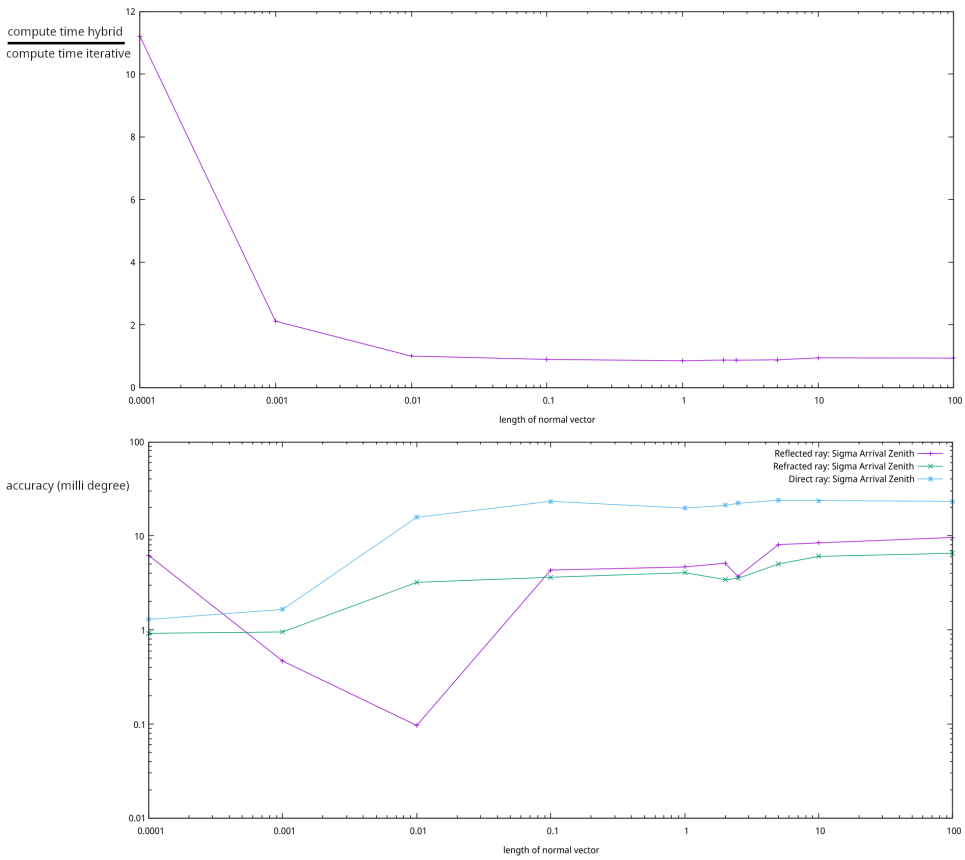

Figure 4.5: influence of the length of the normal vector

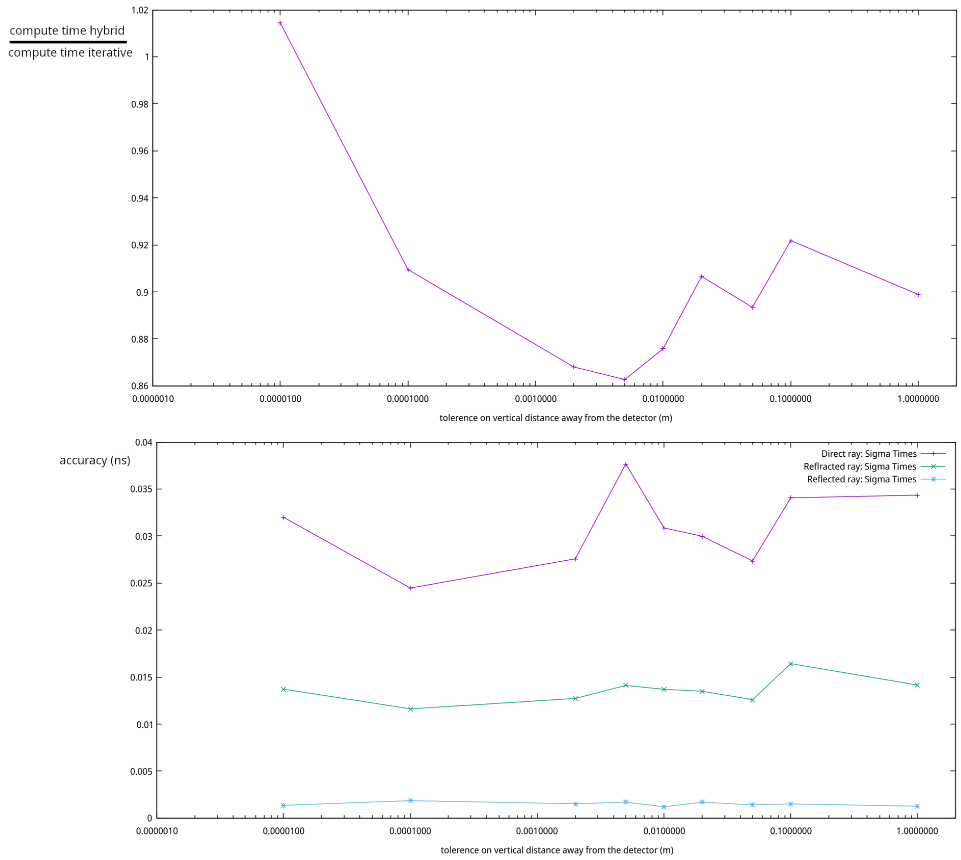

Figure 4.6: influence of the tolerence on vertical distance

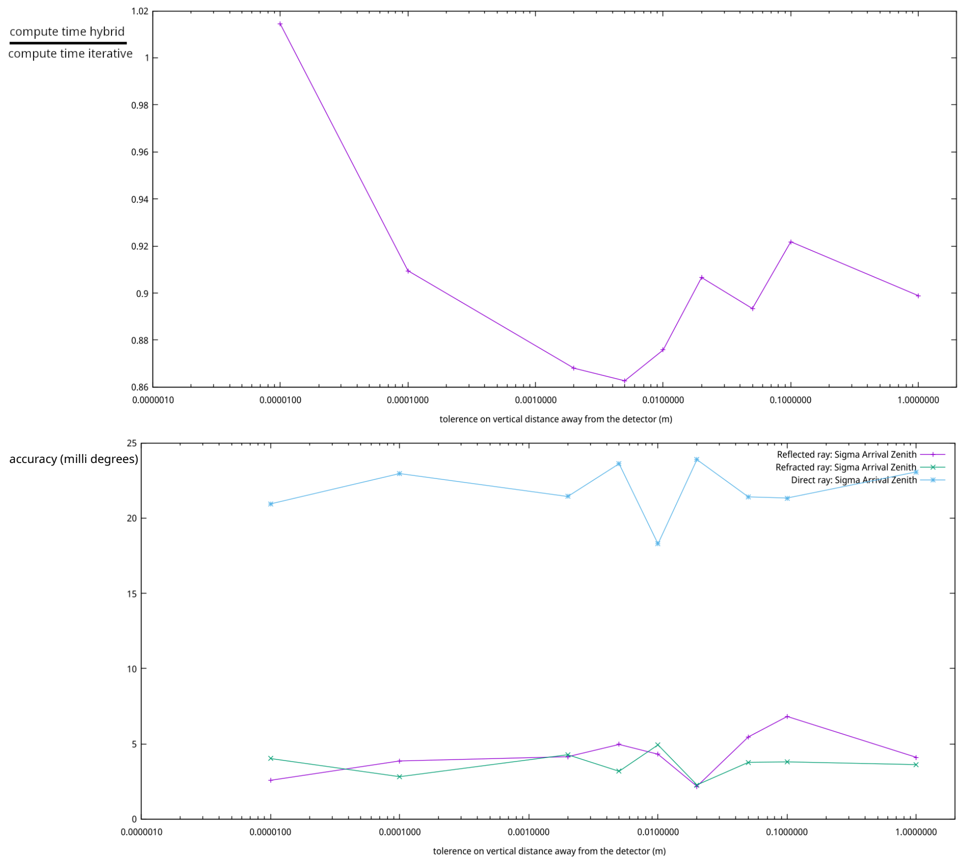

Figure 4.7: influence of the tolerence on vertical distance

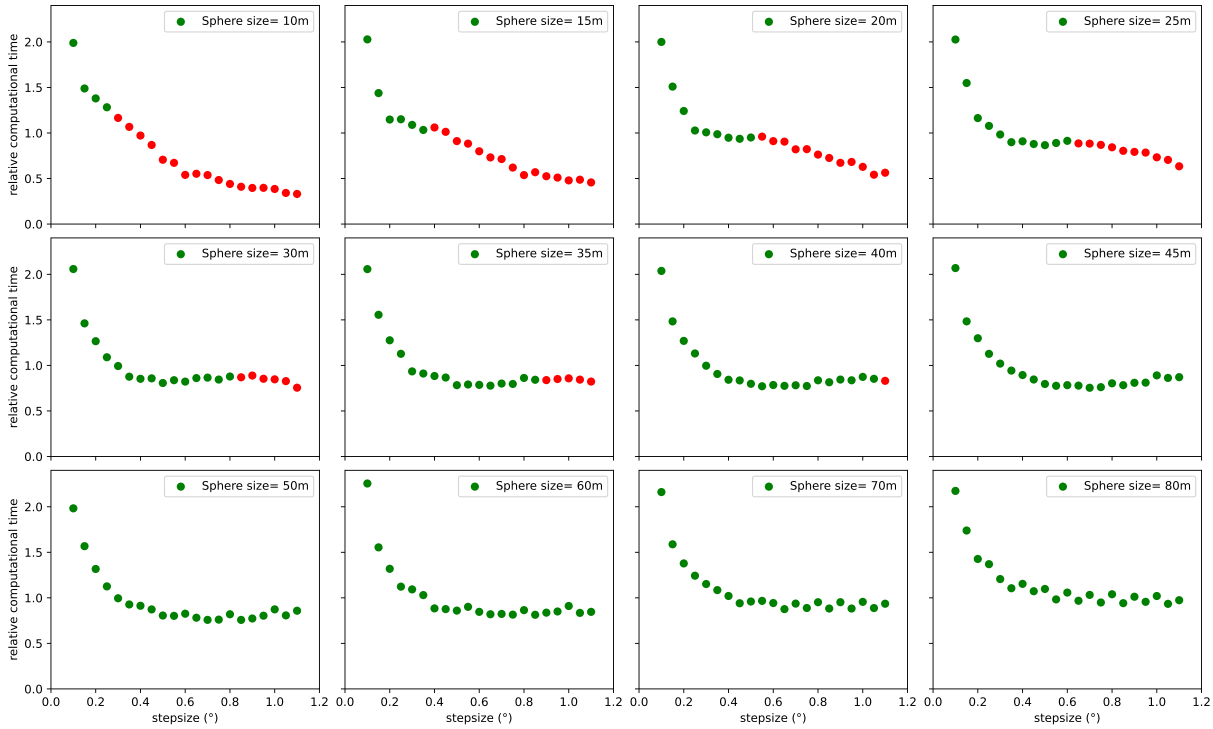

Figure 4.8: Variation in Sphere and angle step size with report on relative time.

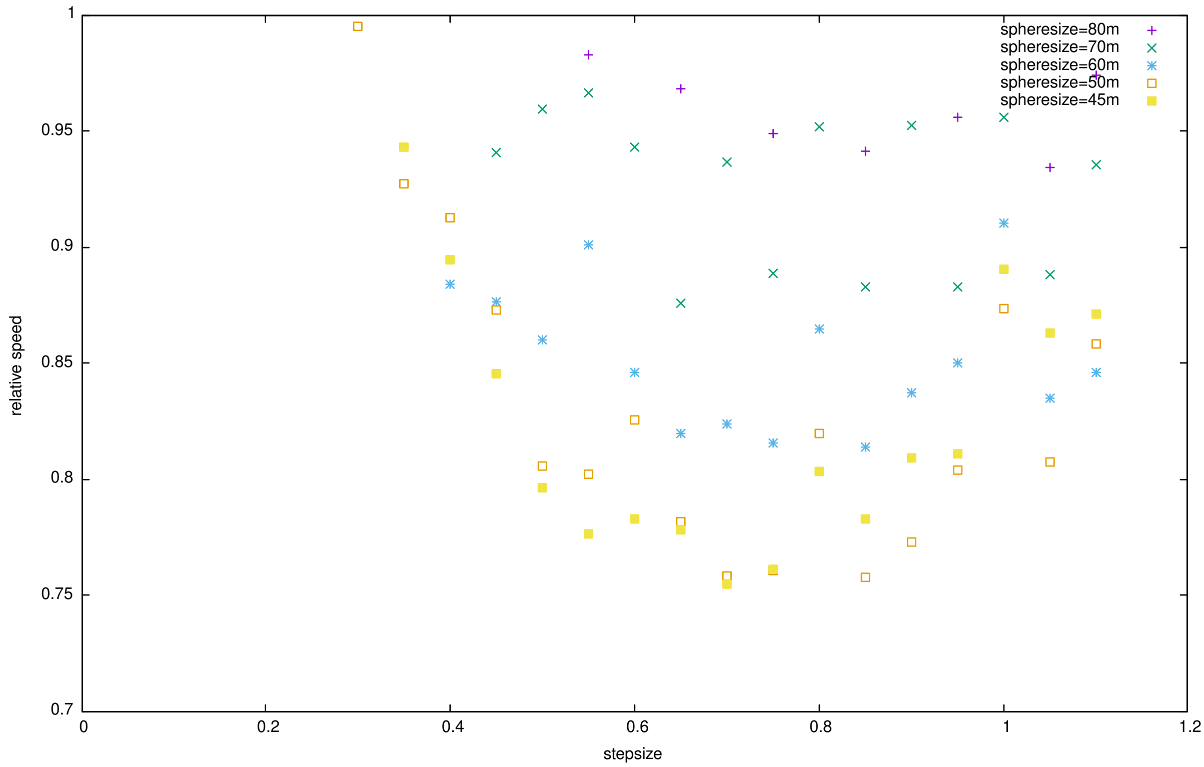

Figure 4.9: Green values in variation in sphere and angle step size with report on relative time.

CHAPTER

5 WEATHER BALLOON

In this chapter we'll simulate radio signals coming from a weather balloon flying over the stations. Our goal is to use the plane waves method to reconstruct the position of the weather balloon with the timing information inferred from the detected radio signals in the detectors. If this is somewhat succesfull it can be used (as we'll get to shortly) to find out the local index of refraction in the ice.

There are 2 changes that need to happen first to our algorithm for us to be able to simulate this: The air observers needs to be hard removed as to make a ray tracing possible from within the air to the detector and second off, we'll need to implement secondaries. The problem is essentially that a ray coming from the balloon propagates to the ice, refracting and reflecting and then one of the refracted rays hits the detector. The "primary" ray is concidered the reflected one so we adjusted the algorithm to look at the secondary that ends closest to the detector and return that ray. What this has as a consequence is that the "path" you get back is only the path from when it "became" a secondary (so only the part below the ice) but this can be easily fixed as the radio wave just propagates straight from the balloon to the beginning of that ray, making the full ray reconstructable by just assuming a line from the balloon to the "start" of the ray.

From this information the propagation time from the balloon to the ice t can later be added to the time of the path in the ice by measuring the length d of the drawn line from the balloon to the beginning of the recorded path, setting the speed of radio waves in air to c and then just adding $t = d/c$.

5.1 Plane Wave Reconstruction

Now having modified our ray tracer, the first problem we'll consider is plane wave reconstruction of the original position, an example path to some of the deep sensors is given in figure 5.1 The plane wave reconstruction can easily be understood using figure 5.2, the waves coming in are drawn in blue and make a certain angle with the detectors. the top detector (top box) detects the wave at a certain time t_1, the bottom detector detects it at a time t_2. In our database, after decoding the signal we'd thus see that these two detectors got a signal $\Delta t = t_1 - t_2$ seconds apart

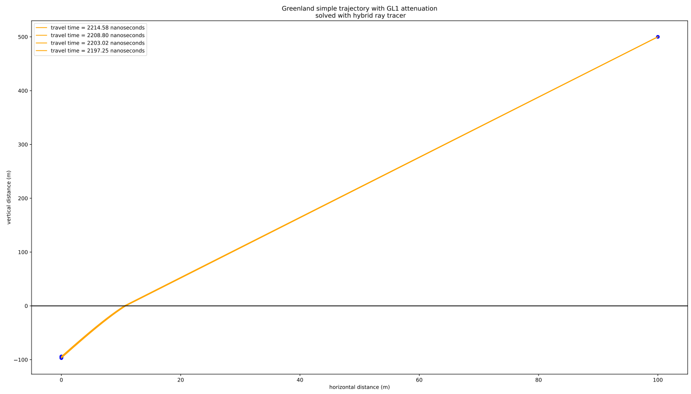

Figure 5.1: Example trajectory of rays coming from a weather balloon (blue dot top right) and going through the ice to the various detectors (blue dots bottom left)

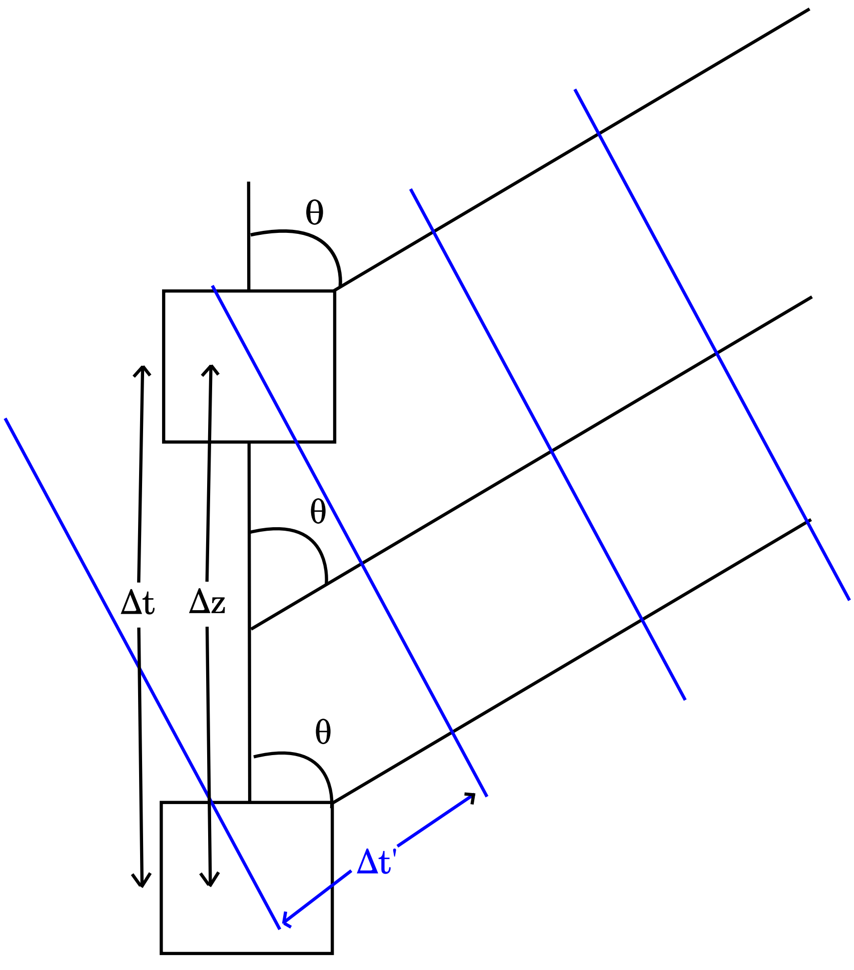

Figure 5.2: Illustration of Plane waves

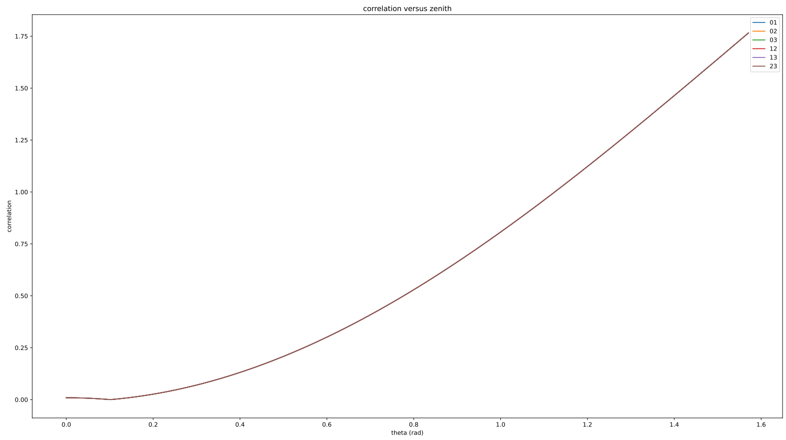

Figure 5.3: Example normed correlation functions

from eachother. Now ideally this is equal to the time $\Delta t'$ which is the time it took the wave to propagate that distance which we can calculate from basic trigonometry and dimensional analysis:

$$\Delta t' = \frac{m}{(m/s)} = (s/m) * m = v^{-1} * m = v^{-1} \cos\theta \Delta z \tag{5.1}$$

With $v = c/n$ the local speed of light. As previously discussed this n is depth-dependent and for comparison with the fitted index we'll be using the models local index of refraction. Say we have 4 detectors at depths -94,-95,-96,-97, this then would mean that we'll set the index of refraction at a depth of -95.5, exactly inbetween:

```
ice = medium.greenland_simple()
n_exact = ice.get_index_of_refraction(np.array[0,0,-95.5])
```

Now in reality we don't know the angle a priori, we'll only have the timing information, so we'll perform a scan by minimizing something we define here as *the correlation function*:

$$Correlation(\theta) := \Delta t - \Delta t' = \Delta t - \frac{\cos\theta \Delta z}{v} \tag{5.2}$$

If we have more than 1 detector however (which of course will be the case in RNO-G), we'll need to specifiy various correlation functions. E.g if we have four detectors labeled 0 to 3 we'll have to construct correlation functions between detectors 0&1, 0&2, 0&3, 1&2, 1&3 and 2&3 . As all of these correlation functions will have different sizes we'll norm them as follows:

$$Correlation_{Normed}(\theta) = \frac{Correlation(\theta)}{\int Correlation(\theta)\Delta\theta} \tag{5.3}$$

An example of these correlation functions is shown in figure 5.3, notice how you can't differentiate between the correlation functions, this is only possible because of the hybrid ray tracer having that high of a precision. After this we can sum them, as shown in figure 5.4, and look where it reaches it's minimum. Using this angle we can then reconstruct a ray and guess where the weather balloon is approximately, this is illustrated in figure 5.12.

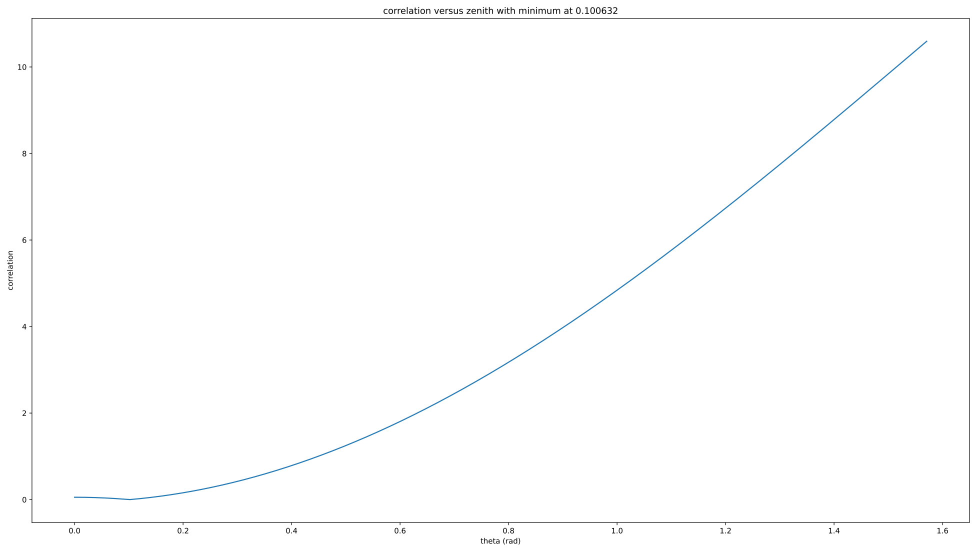

Figure 5.4: Example sum of the normed correlation functions

5.2 Is the goal feasible?

In the example reconstruction illustrated in figure 5.12 the difference in angle between direct to balloon and plane wave reconstruction is already quite small (0.65329617%) but as the balloon gets closer to the detector this reduces significantly as is shown in figure 5.13 where the difference in angle between direct to balloon and plane wave reconstruction is only 0.06788141%. Our goal is to find the local index of refraction n by using the plane wave reconstruction with the recorded timing and the positional data from the weather balloon as the plane wave reconstruction is heavily dependent on the index of refraction (as can be seen in equation 5.2). As was already established we'll consider the index of refraction in the middle of all the detectors (instead of a different one for every pair of detectors), after experimenting this doesn't seem to have an impact on the accuracy of the plane wave reconstruction.

Now let's ask ourselves the question, within which angles should the weather balloon fly for the data to be useful? As was previously stated, the further the weather balloon is away (in the x direction) the bigger the zenith angle with the detector the less accurate the plane wave reconstruction. So which angles are acceptable? Note that not only angle but also height will eventually play a role in the accuracy, the angle however gives a good starting point. To determine this our method works as follows:

we vary the position of the weather balloon in the x direction (keeping the height constant), simulate the ray path to the channels 0 to 3 and then fit n such that the difference between the reconstructed angle (from the plane wave method) and the direct angle (angle between the middle of channels 0-3 and the balloon) is the smallest possible. Then we compare the n we have fit to the one we know from the model at that position. We quantise the discrepency between these two indices of refraction using what we here define as the *relative accuracy*:

$$\varepsilon\ (\%) = \frac{n_{\text{fit}} - n_{\text{exact}}}{n_{\text{exact}}} \times 100 \tag{5.4}$$

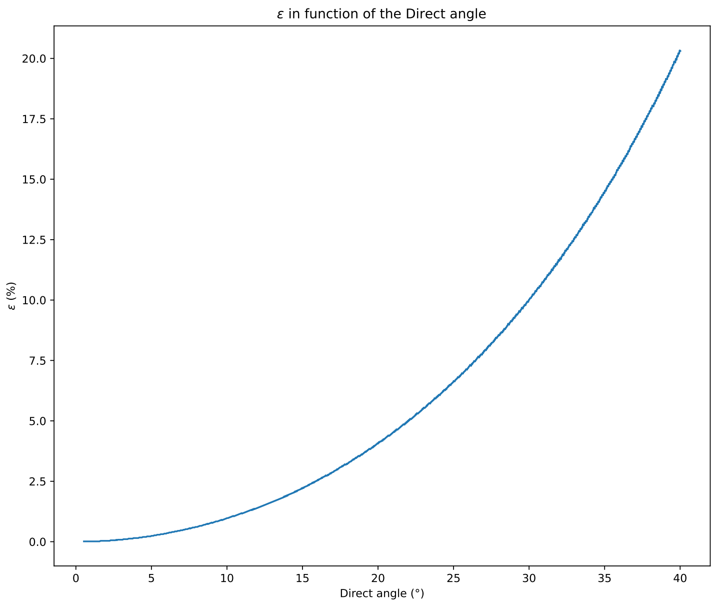

Figure 5.5: Epsilon in function of the direct angle

Carrying this out[1] we get figure 5.5, i.e it gets exponentially shifted towards higher n as the balloon moves further away. If we wish our accuracy to be within 1%, the angle the balloon makes with the middle of channels 0 to 3 needs to be less than 10°. An example path of a weather balloon is shown in figure 5.11, looking specifically at the height information recorded by the weather balloon in a .root file using ROOT[2] we get what is shown in figure 5.6. It can be seen that the elevation varies between 3228m (read the graph as: Over a 1000 data entries at that height) and 22755m (entries go to zero after that height). This is relative to sea-level, looking at the height map of greenland as shown in figure 5.7 this is obvious. It's quite difficult to work directly with the global geographic coordinate system (longitudinal, latitude and elevation coordinates), that's why we convert them to local ENU coordinates (north, east, up) relative to

[1]The code for this can be found in projects-mt/BaLLooN/simulations as plane_wave.py
[2]https://root.cern/

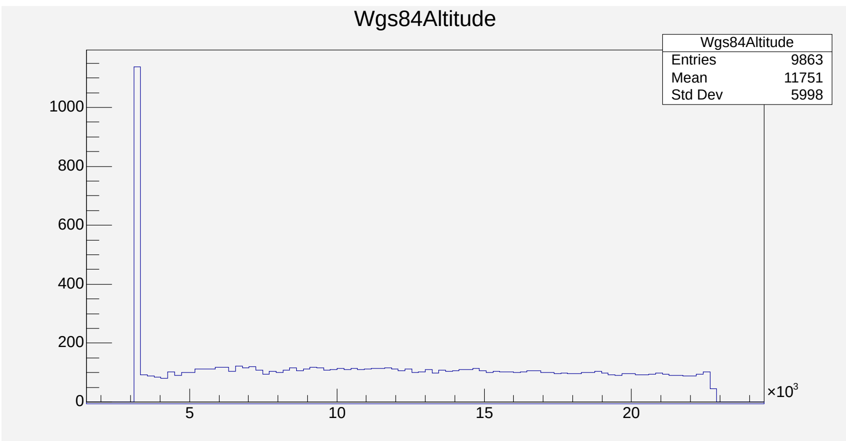

Figure 5.6: Height data viewed in ROOT

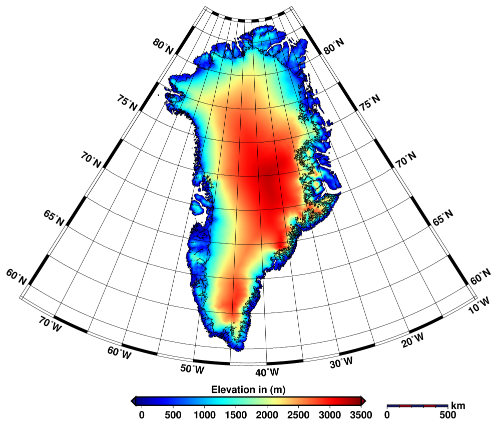

Figure 5.7: Height map of greenland

the 'DISC' which is located at 72.58279265212887 latitude, -38.45581495328228 longitude and 3251.9489147560234 elevation.

Now what would our <10° policy entail? And is it even possible? Say we take a look at station Terianniaq (station 12) it's located at 72.6000868058195° N -38.4962265332872° W. converting this into ENU coordinates we get -137.67250176003688N 1727.5184983294744E, we then set our "up" to be -95.5m as this is the approximate location of the middle of channels 0-3. Now looking at e.g the Balloon path recorded on the 20th of august 2022 (figure 5.10) we see that the balloon crosses paths closely with detector 12, but how close was this encounter? To quantize this we can take a look at every data entry (there are >12000 entries) individually and compute the angle the balloon makes with the detector by first converting the location of the balloon in ENU coordinates, then calculating the horizontal distance ($\sqrt{(x-x')^2+(y-y')^2}$) then the relative vertical distance $|z-z'|$ and then from those compute the angle ($tan(\theta) = \frac{Hor.}{Vert.}$) doing this and recording when the balloon gets close enough to get below the 10° mark we get figure 5.9. We thus see that in this example the $< 10°$ policy is viable.

Now how much data do we have that way? We'll be looking at the data recorded over the summer of 2022, more particularly 15/06/2022 - 30/09/2022. The positional data of the weather balloons was obtained from the `ftp1.esrl.noaa.gov` website using the rno-g-sonde script of the official RNO-G github page .After looping through every weather balloon gpx file recorded in the summer of 2022 and seeing where it get's within 10 degrees we get the data shown in appendix B, even though this is quite a lot of data there's still another step that we could do to broaden the amount of usable data.

5.2.1 Refraction at the surface

Up until now we have not used the property that waves refract at the surface as we didn't want to assume anything, now say that we include refraction at the surface for our plane wave reconstruction. This would mean that we'd follow analogous steps as our previous analysis, i.e doing a plane wave reconstruction from the difference in timing and trying to fit the index of refraction, only now the plane wave abides with snell's law at the surface, going from n=1.27 to n=1 and we'll need to minimize the horizontal distance from the ray at the height of the balloon and the balloon, not the angle. The full algorithm thus goes as follows: We first reconstruct the plane wave launch angle θ_1 by minimizing the correlation function previously defined, this gives us a function

$$z = a_{InIce} * x + b_{InIce} \tag{5.5}$$

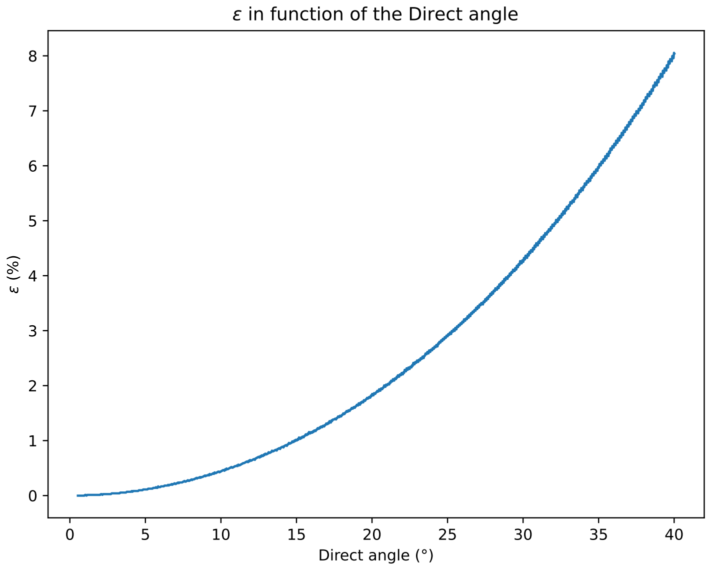

Figure 5.8: epsilon IFO possible angles from channels 0-3 with refraction at the surface

The outgoing zenith angle at the surface θ_2 can be calculated from snell's law:

$$n_1 \sin\theta_1 = n_2 \sin\theta_2 \implies \theta_2 = \sin^{-1}\left(\frac{n_1}{n_2}\sin\theta_1\right) \tag{5.6}$$

from this we know the slope of the wave path $a_{InAir} = \tan\left(\frac{\pi}{2} - \theta_2\right)$ but not the offset, but this can easily be found from equation 5.5 as

$$z = 0 = a_{InIce} * x_{End} + b_{InIce} \implies x_{End} = -\frac{b_{InIce}}{a_{InIce}} \tag{5.7}$$

and

$$z = 0 = a_{InAir} * x_{End} + b_{InAir} \implies b_{InAir} = -a_{InAir} * x_{End} \tag{5.8}$$

$$= a_{InAir} * \frac{b_{InIce}}{a_{InIce}} \tag{5.9}$$

Now that we have the function describing the "path of the plane wave"[3] in the air we can find out the horizontal position at the height of the balloon as

$$z = z_{Balloon} = a_{InAir} * x_f + b_{InAir} \implies x_f = \frac{z_{Balloon} - b_{InAir}}{a_{InAir}} \tag{5.10}$$

and iteratively loop over possible indices of refraction, minimizing $|x_{Balloon} - x_f|$.

Doing this whilst looping over possible horizontal balloon positions, we get the result shown in figure 5.8[4] As you can see we can now go up to 15° and still have less than 1% error! The only drawback of this method is that we need to assume the index of refraction to be 1.27 at the surface of the ice, if this isn't the case in some places our predictions won't be accurate.

[3] we use double quotes as to emphasize that this is a reconstruction method and not an actual wave
[4] The code for this can be found in projects-mt/BaLLooN/simulations as plane_wave_with_snell.py

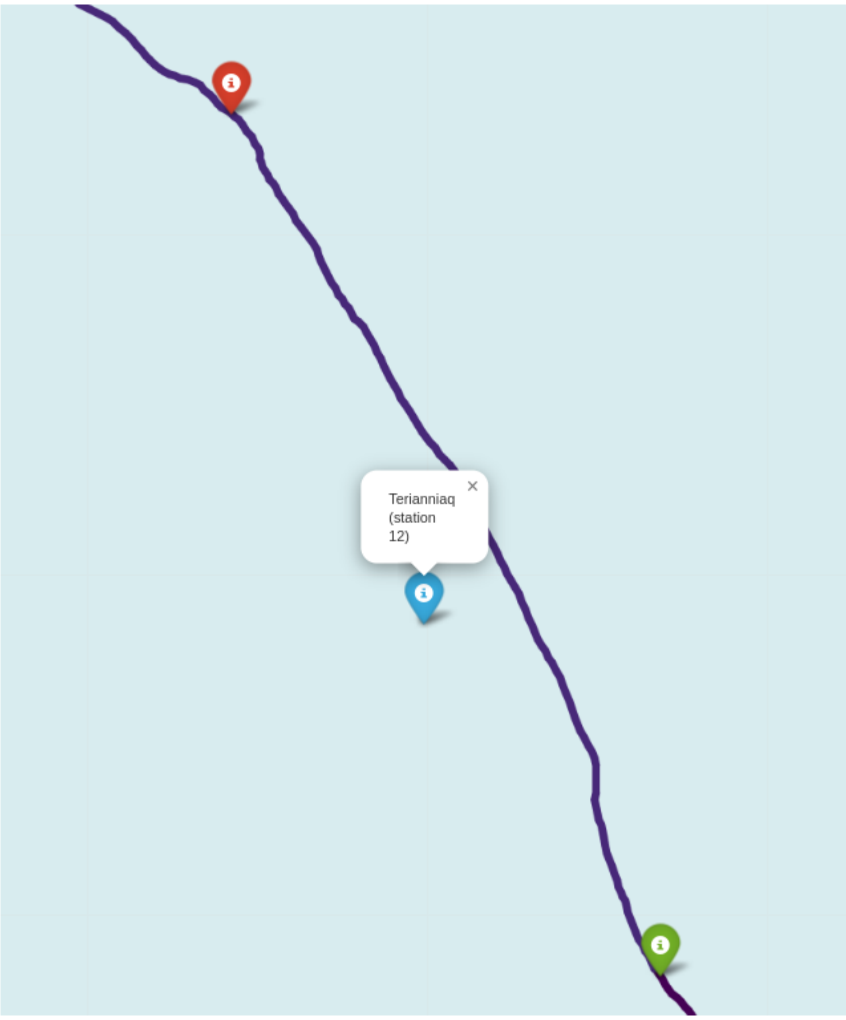

Figure 5.9: Illustration of when the angle with the deep array (channels 0-3) with the weather balloon is less than 10 degrees, the green mark indicates when it starts being less than 10 degrees and the red mark when it stops being less than 10 degrees.

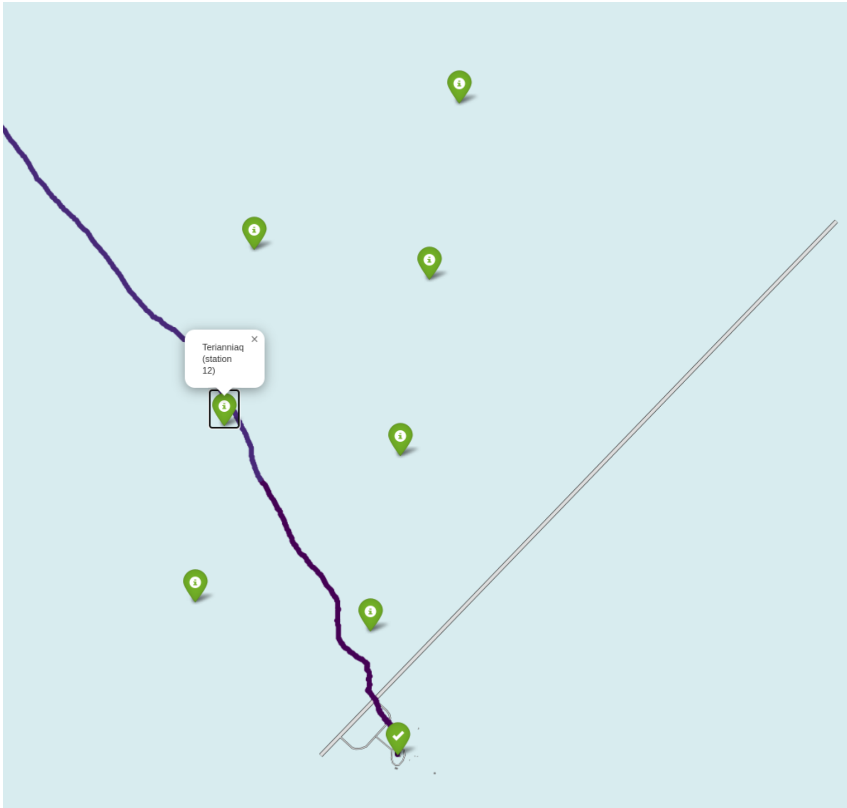

Figure 5.10: Path traced out by a weather balloon released at 20/08/2022

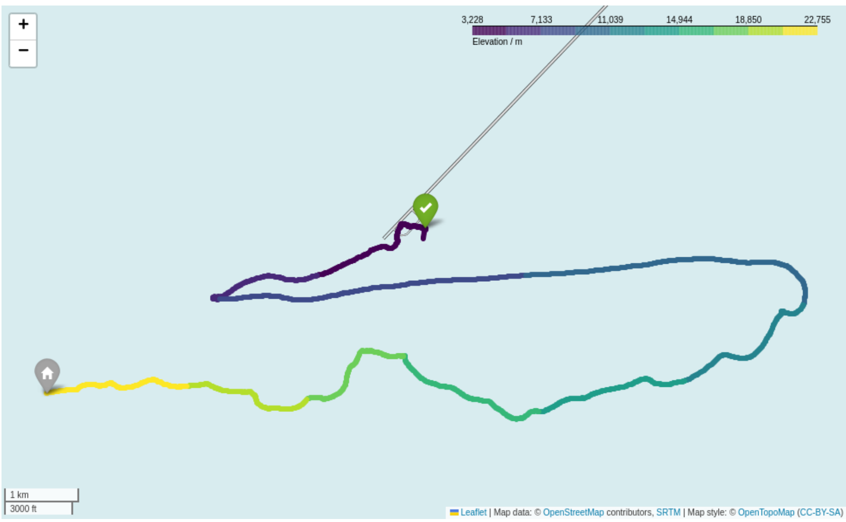

Figure 5.11: Path traced out by a weather balloon released by Bob Oeyen, the checkmark indicating the start and the house mark the end

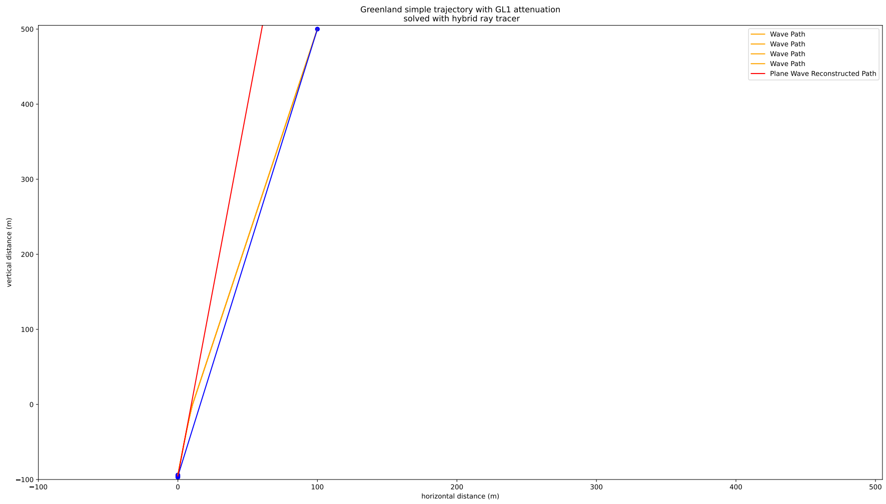

Figure 5.12: Example plane wave reconstruction of weather balloon position

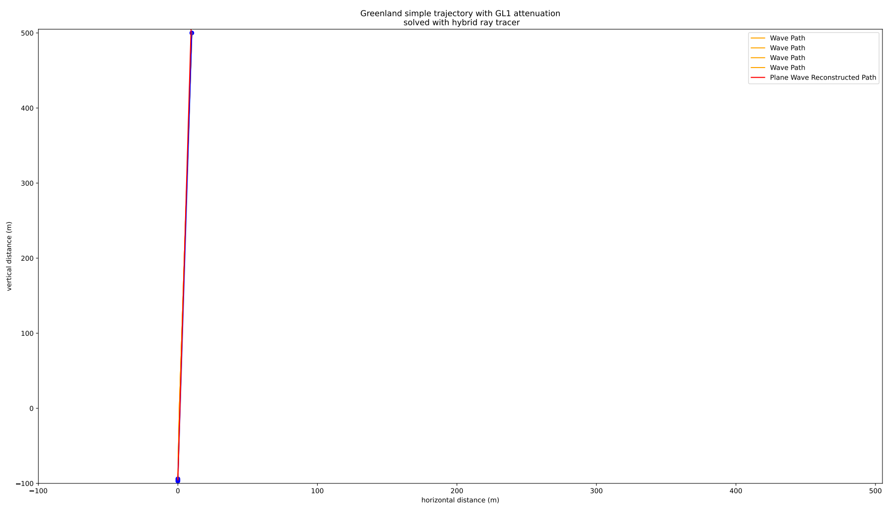

Figure 5.13: Example plane wave reconstruction of near-flying weather balloon position

5.3 Error on prediction

Running ahead on the actual measurements, let's estimate how accurate our predictions will be (in the non-snell case). For the moment we're only interested in the deep channels 0-3. Let's label the vertical spatial accuracy, i.e how accurately we know the height of these channels, δz[5]. And the timely accuracy, or how accurate the vpol timing characteristics are, δt. If we want to fit n, we first minimize the summed correlation function to construct the plane wave. One correlation function is given by

$$Correlation(\theta) := \Delta t - \Delta t' = \Delta t - \frac{\cos\theta \Delta z}{v} \tag{5.11}$$

Say the minimum occurs at $Correlation(\theta) = Correlation(\theta_{min}) := \mathcal{C}$, we can then re-write this equation for n:

$$n = \frac{c(\Delta t - \mathcal{C})}{\cos\theta_{min}\Delta z} = \frac{c}{\cos\theta_{min}}\left[\frac{\Delta t}{\Delta z} - \frac{\mathcal{C}}{\Delta z}\right] \tag{5.12}$$

The Δz is the vertical distance between two channels and thus has an error of $2\delta z$ and Δt is the time difference between two channels, implying an error $2\delta t$. Let's look at the two terms seperately (assuming the error on θ_{min} to be negligable), the first quotient $\phi_1 := \Delta t/\Delta z$ has a variance [12] of

$$s^2_{\phi_1} = \frac{1}{\Delta z^2}s^2_{\Delta t} - 2\frac{\Delta t}{\Delta z^3}s_{\Delta t \Delta z} + \frac{\Delta t^2}{\Delta z^4}s^2_{\Delta z} \tag{5.13}$$

Assuming Δt and Δz to be independent:

$$s^2_{\phi_1} = \frac{1}{\Delta z^2}s^2_{\Delta t} + \frac{\Delta t^2}{\Delta z^4}s^2_{\Delta z} \tag{5.14}$$

$$= 4\left(\frac{1}{\Delta z^2}\delta t^2 + \frac{\Delta t^2}{\Delta z^4}\delta z^2\right) \tag{5.15}$$

And the second term ($\phi_2 := -\mathcal{C}/\Delta z$):

$$s^2_{\phi_2} = \frac{\mathcal{C}^2}{\Delta z^2}s^2_{\Delta t} \tag{5.16}$$

$$= 4\frac{\mathcal{C}^2}{\Delta z^2}\delta t^2 \tag{5.17}$$

$$\tag{5.18}$$

Our uncertainty on the index of refraction is thus (neglecting unknown systematic errors):

$$\delta n = 4\left(\frac{c}{\cos\theta_{min}}\right)\left(\frac{1}{\Delta z^2}\delta t^2 + \frac{\Delta t^2}{\Delta z^4}\delta z^2 + \frac{\mathcal{C}^2}{\Delta z^2}\delta t^2\right) \tag{5.19}$$

If we have more than 2 detectors, say N then the uncertainty on the fit can be assumed to be the RMS of the individual uncertainties:

$$\delta n = \sqrt{\sum_{i=0}^{N}\delta n_i^2} \tag{5.20}$$

Let's assume ϵ to be an absolute error. Now due to this inherent inaccuracy, the "global" uncertainty on n also has an additional error of $\pm\epsilon(\vec{r})n$ with $\vec{r}$ the position of the balloon. Our final error on n is thus:

$$\delta n(\vec{r}) = \epsilon(\vec{r})n + \sqrt{\sum_{i=0}^{N}\left[4\left(\frac{c}{\cos\theta_{min}}\right)\left(\frac{1}{\Delta z_i{}^2}\delta t^2 + \frac{\Delta t_i{}^2}{\Delta z_i{}^4}\delta z^2 + \frac{\mathcal{C}^2}{\Delta z_i{}^2}\delta t^2\right)\right]^2} \tag{5.21}$$

[5]meaning if we have a measurement z_i the true value is within $z_i \pm \delta z$ with 95% certainty

If we assume the ϵ to overestimate the index of refraction the same way in real life as in the simulation however, our estimated n can be corrected as

$$n_{\text{corrected}}(\vec{r}) = \frac{n(\vec{r})}{\epsilon(\vec{r}) + 1} \tag{5.22}$$

and our error becomes only the second part of equation 5.21. As the error on the position of the channels is not yet fully known this whole section mainly serves as a future reference to calculate the errors on the indices of refraction that will be calculated in the next sections within this chapter.

Figure 5.14: Close encounter between a weather balloon and detector 23 on the 29th of august 2022 at 11:18

5.4 Fitting the index: Channels 6 and 7

Now that we know our goal to be feasible, let's analyse some data. As we'll start by just analysing one event, let's take one of the best events possible for our analysis. A close look at graph 5.5 shows that events under 5° produce an error of less than 0.22%, implying that if we measure n to be 1.7407 our error will only be 0.0038. After looping through all the balloon positional files and only outputting the < 5 ones we get some moments where balloons were actually close enough (note that < 5 almost never happens at low heights).

If we search in the DESY database [6] within the calculated timeframes for the particular detectors where the balloon gets close enough to, AND where the 403MHz signal coming from the Ballon (see figure 5.19) is detected in the deep channels, the events of the 29th of august stands out; between 11:18:46 and 11:18:56, the balloon gets really close to detector 23 as can be seen on figure 5.14. If we take a look at the detected signals we see that at run 691 the event 489 gets recorded at 2022-08-29 11:18:32+00:00 showing a clear 403MHz peak at channels 5-7. It is of course unfortunate that we don't get to measure the index of refraction at the deep component jet but a quick calculation shows that if we measure the index of refraction using detectors 5 and 6 (getting the index of refraction at -70m) the error will be $\approx 0.5\%$ which is a nice start[7].

Now to calculate the differences in timing for this received signal, the code used for this is called FitN.py and stored at the repository https://github.com/arthuradriaens-code/projects-mt.git under BaLLooN/RealData, let's go over the full code step by step:

5.4.1 Spatial data

The first part we'll need to concern ourselves with is determining the relative positions of everything. The balloon data file and the time when the event took place are given, from these two both the latitudenal and longitudinal position and elevation of the balloon at the given time is determined. We convert these three measurements to the ENU coordinate frame and store it in the array *BalloonPosition*. The next step is to get the location of the detector, for this we first instantiate a detector object

```
det = NuRadioReco.detector.detector.Detector(json_file="RNO_season_2022.json")
```

[6] https://rnog-monitor.zeuthen.desy.de/

[7] This calculation was performed with the program CalculateInherentErrorWithSnell.py located in projects-mt/BaLLooN/RealData

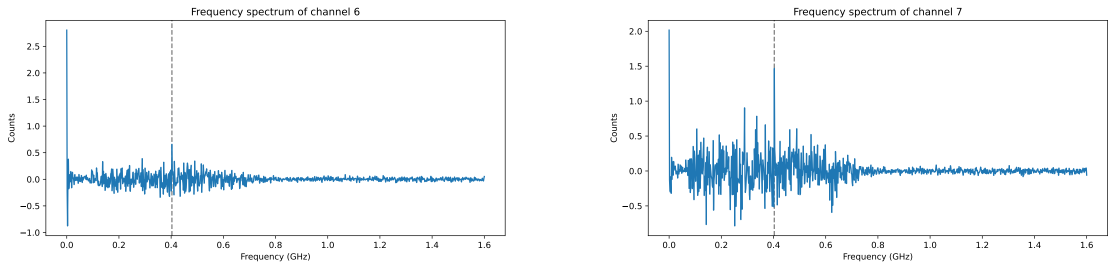

Figure 5.15: recorded frequencies on detector 23 at 2022/08/29 11:18:32

The RNO season 2022 json file can be found on the official RNO-G github under "analysis-tools", then we "update" the detector to the event time and get the absolute position of our detector (station 23) via the get_absolute_position module:

```
        stationlocation = det.get_absolute_position(station_id)
```

Now that we have both the position of our balloon and station 23 in ENU coordinates, let's make the calculations simpler by setting the detector as the central coordinate. i.e our new balloon position will be

$$RelBalloon = BalloonPosition - station \tag{5.23}$$

And as we might want to plot this later, due to the cylindrical symmetry, we can rotate the coordinates to get rid of our y-axis. We can do this by defining the radius:

$$r := \sqrt{RelBalloon_x^2 + RelBalloon_y^2} \tag{5.24}$$

and just setting this equal to $Balloon_x$ and setting $Balloon_y$ to zero (equivalent to setting $\theta = 0$ in a rotation).

Now we don't have the position of our individual channels yet, only of the station itself, these can however easily be obtained using the get_relative_position module on our detector object, as we chose our station to be the center of the coordinate system, these relative positions are absolute positions in our frame of reference.

5.4.2 Signal analysis and initial guesses

Now that we have our geometry, let's analyse the data for the channels 6 and 7, the data for a particual channel is stored in a channel object. From this object we can get the recorded voltages with the get_trace() module, the recorded times with the get_times() module, the recorded frequencies with the get_frequencies() and the recorded spectrum corresponding to these frequencies with get_frequency_spectrum() , note that the last two do a FFT on our data. The recorded spectrum of both channels is given in figure 5.15, we observe a clear spike at 403MHz.

We know that the signal sent out by the weather balloon has a frequency of 403MHz. As the data is measured in nanoseconds the frequency is:

$$f = 403\text{MHz} = 403 \times 10^{-3}\frac{1}{\text{ns}} \tag{5.25}$$

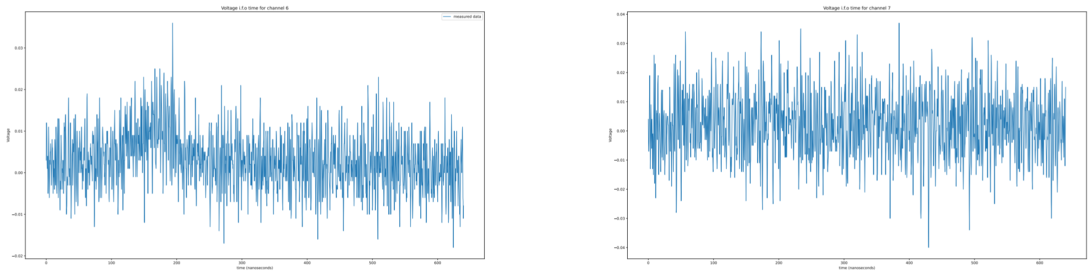

Figure 5.16: recorded voltage i.f.o time on detector 23 at 2022/08/29 11:18:32 for channels 6 and 7

but looking at the data in figure 5.16 we see that we'll have to do some processing before fitting a sine of the form

$$\mathcal{S} = A \cdot \sin\left(\omega t + T\right) \tag{5.26}$$

with

$$\omega = 2\pi f \tag{5.27}$$

Let's first pass this signal through a sixth order butterworth filter with a passband of [0.4031249, 0.4031251][8]. Doing this we notice that the signal looks as shown in figure 5.18, where it's clear that even though the balloon indeed sends out a sinusoidal 403MHz frequency, this signal is amplitude modulated (AM). Meaning that we have a sinusoidial carrier signal $c(t)$:

$$c(t) = A\sin(2\pi f_c t) \tag{5.28}$$

with a message signal

$$m(t) = Am\cos(2\pi f_m t + \phi) \tag{5.29}$$

These two modulated together thus has the form

$$V(t) = \left[1 + \frac{m(t)}{A}\right] c(t) = A\sin(2\pi f_c t)[1 + m\cos(2\pi f_m t + \phi)] \tag{5.30}$$

With a little correction that, due to the nature of observing the signal, there will be another phase:

$$V(t) = A\sin(2\pi f_c t + \phi_1)[1 + m\cos(2\pi f_m t + \phi_2)] \tag{5.31}$$

Herein the carrier frequency is given by $f_c = 0.403125$ as previously established but with the other parameters seemingly unknown which we'll have to fit to the measured data. We can, however, do some educated guesses which will help the fitting algorithm. The first guess we'll do is establish the maximum value, as we have implemented an algorithm of finding the envelope functions (in green and orange on figure 5.18), this is as simple as calling the max function on the high envelope. Looking at our function this max value corresponds to

$$e_{highmax} = A(1 + m) := E_1 \tag{5.32}$$

The minimal value of our high envelope function corresponds to the minimal value of the message signal, due to symmetry it's actually easier to just look at the absolute maximal values of the low envelope:

$$|e_{lowmax}| = A(1 - m) := E_2 \tag{5.33}$$

[8]This is a filter that only let's frequencies pass whom are within the passband

combining these two we get an equation for A and one for m:

$$m = \frac{\frac{E_1}{E_2} - 1}{\frac{E_1}{E_2} + 1} \tag{5.34}$$

$$A = \frac{E_1}{1+m} \tag{5.35}$$

$$\tag{5.36}$$

The frequency of the message signal can also be found from looking at the difference between subsequent "bumps", these will be spaced some time T apart, from which an initial guess for the message frequency can be found as $f_m = 1/T$. The only thing left to find is the phases ϕ_i, we'll just fit these with an initial smart guess, for which I'll first have to talk about cable delays which we'll denote as t^d. We get the delay for the individual channels with the get_cable_delay module, these later on need to be substracted from the fit.

The difference in timing can be found from using the different ϕ's we will fit; this is easy to see from the following example: Consider a sine wave

$$sin(\omega t) \tag{5.37}$$

This reaches a certain value x after a time t_x:

$$t_x = \frac{1}{\omega} \sin^{-1}(x) \tag{5.38}$$

Now a sine wave with an offset of $-\phi$

$$sin(\omega t - \phi) \tag{5.39}$$

reaches this same x only after a time

$$t_x = \frac{1}{\omega} \left(\sin^{-1}(x) + \phi\right) \tag{5.40}$$

i.e a difference of ϕ/ω.

Knowing this relationship is useful for finding an initial guess for ϕ as the recorded travel times T_i are of the form $T = -\phi/\omega - t^d$ and we know that the travel times should be around 4200 ns from a simple simulation using the greenland simple ice model, meaning that our guess for ϕ is in the neighborhood of $-\omega(4200 - t^d)$ and should give the smallest correlation function; doing this for this example we get that the ϕ for channel 6 should be -752 and channel 7 we give as initial guess the final fit of channel 6 as it is higher and will thus have less travel time implying a higher ϕ (the algorithm fits the ϕ upwards). Fitting this function with the initial guesses you get what's shown on figure 5.17, i.e a perfect fit on the data.

5.4.3 Difference in timing

The signals detected in the channels have the form

$$V(t) = \sin(\omega_c t + \phi_c)\,[1 + m\cos(\omega_m t + \phi_m)] \tag{5.41}$$

$$= \sin(\omega_c(t + \phi_c/\omega_c))\,[1 + m\cos(\omega_m(t + \phi_m/\omega_m))] \tag{5.42}$$

$$:= \sin(\omega_c(t + T_c))\,[1 + m\cos(\omega_m(t + T_m))] \tag{5.43}$$

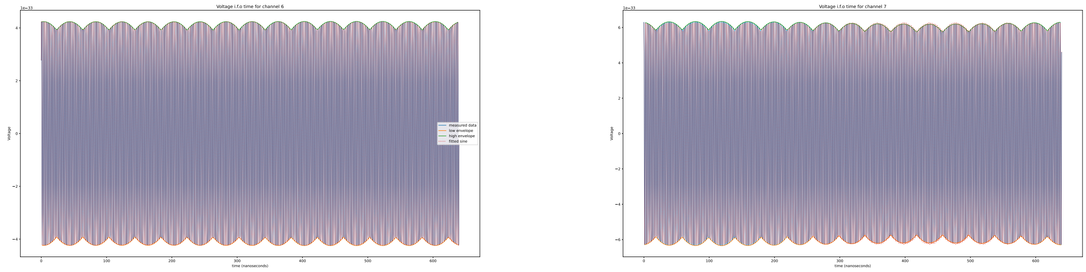

Figure 5.17: recorded voltage i.f.o time on detector 23 at 2022/08/29 11:18:32 for channels 6 and 7

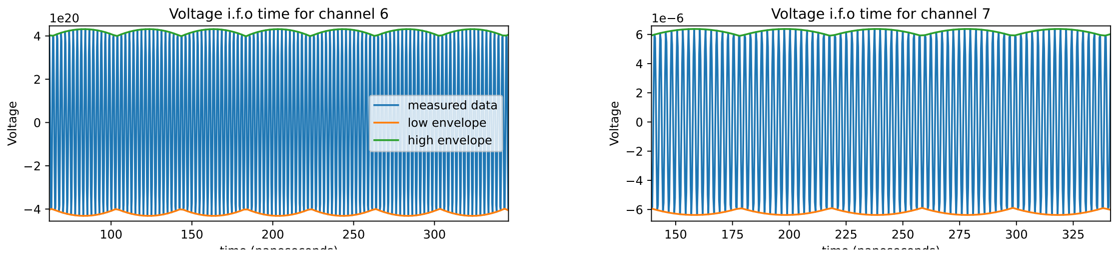

Figure 5.18: recorded voltage i.f.o time on detector 23 at 2022/08/29 11:18:32 for channels 6 and 7

Now, for the plane wave reconstruction, we want to know the difference between the arrival times for channels 6 and 7. We take it to be sufficient to let the offset in time be the offset on the message as the offset on the carrier is sufficiently small, i.e

$$\Delta T := T_6 - T_7 = T_6^m - T_7^m \tag{5.44}$$

our actual difference in timing is thus:

$$t_6 - t_7 = T_6 - T_7 - (t_6^d - t_7^d) = \Delta T - (t_6^d - t_7^d) \tag{5.45}$$

Now going through the full calculation we get that the index for refraction at a depth of 47.714m is 1.6061, which is a fairly good estimate as, looking at the measurements depicted in figure 2.5 a depth of 47.7m would correspond to a density of about $710kg/m^3$, using Schytts equation this would thus give an index of refraction of 1.603. Now using the positional data we can calculate the relative accuracy ϵ which comes to be about 0.39%. Our final answer is thus: Which has

depth	station number	run used	event_id used	channels used	n
-47.714m	23	691	489	6,7	1.606 ± 0.006

the expected answer within the margin of error. We are aware that this event also shows a peak in the frequency spectrum for channel 5 but the data deviates slightly from an AM signal and thus didn't seem to be usable.

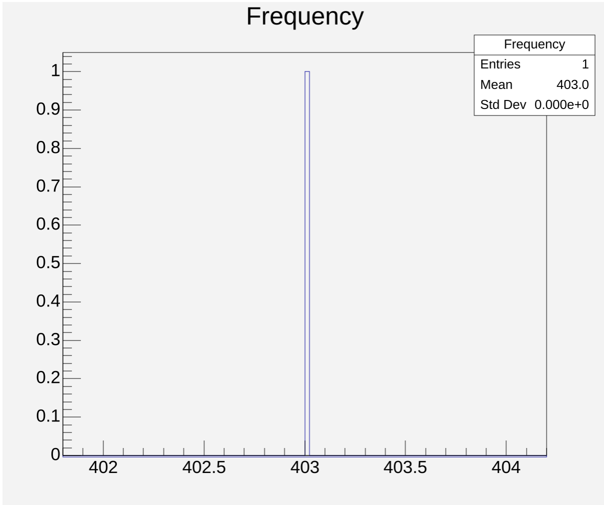

Figure 5.19: Frequencies sent out by the weather balloon

5.5 Fitting the index: deep components

5.5.1 Station 24 run 646 event 373

Going through the full calculation again, i.e getting the relative balloon position and detector positions, fitting the AM function[9] and thus finding the time offsets, minimizing the correlation function for every index of refraction n whilst recording the difference between the path and the weather balloon location and finally returning the index of refraction for which this difference is the smallest; we get as an index of refraction from fit at a depth of -96.1265m : 1.7648612972259445, if we now calculate the theoretical value (for a greenland simple ice model) of the *relative accuracy* ϵ we get 3.3693085783550876%. This thus implies a value of

$$n = 1.765 \pm 0.059 \tag{5.46}$$

It is quite unfortunate that the uncertainty is that large. Now how does this compare to the expected value from density measurements? Looking at the density measurements shown in figure 2.5 we expect a density of about 860 kg/m^3 at a depth of 96.13m, using Schytt's equation with $\rho_0 = 917$ this implies an index of refraction of about 1.73 which is within our confidence interval.

[9]The guess for ϕ to reach $\approx$ 6670ns

APPENDIX

A

LIST OF ABBREVIATIONS

- **AM**: **A**mplitude **M**odulated
- **CMB**: **C**osmic **M**icrowave **B**ackground
- **FFT** **F**ast **F**ourrier **T**ransform
- **GRBs**: **G**amma-**R**ay **B**ursts
- **RNO-G**: **R**adio **N**eutrino **O**bservatory in **G**reenland
- **UHE**: **U**ltra **H**igh **E**nergy

APPENDIX

B

BALLOON PASSBYS UNDER 10° IN THE SUMMER OF 2022

Balloon filename (gpx)	station	expected timeframe
SMT_20220719_231514.gpx	21	2022-07-19 23:19:46+00:00 till 2022-07-19 23:20:41+00:00
SMT_20220719_231514.gpx	11	2022-07-19 23:22:44+00:00 till 2022-07-19 23:27:19+00:00
SMT_20220831_111419.gpx	11	2022-08-31 11:16:20+00:00 till 2022-08-31 11:16:26+00:00
SMT_20220625_111630.gpx	21	2022-06-25 12:22:22+00:00 till 2022-06-25 12:40:57+00:00
SMT_20220625_111630.gpx	12	2022-06-25 12:25:55+00:00 till 2022-06-25 12:45:40+00:00
SMT_20220625_111630.gpx	11	2022-06-25 12:25:58+00:00 till 2022-06-25 12:45:09+00:00
SMT_20220625_111630.gpx	13	2022-06-25 12:26:44+00:00 till 2022-06-25 12:45:40+00:00
SMT_20220625_111630.gpx	22	2022-06-25 12:22:25+00:00 till 2022-06-25 12:42:40+00:00
SMT_20220625_111630.gpx	23	2022-06-25 12:24:10+00:00 till 2022-06-25 12:43:09+00:00
SMT_20220625_111630.gpx	24	2022-06-25 12:26:32+00:00 till 2022-06-25 12:42:24+00:00
SMT_20220826_113003.gpx	21	2022-08-26 11:32:04+00:00 till 2022-08-26 11:32:42+00:00
SMT_20220826_113003.gpx	13	2022-08-26 11:37:48+00:00 till 2022-08-26 11:39:40+00:00
SMT_20220626_112912.gpx	11	2022-06-26 11:35:52+00:00 till 2022-06-26 11:37:32+00:00
SMT_20220808_231507.gpx	11	2022-08-08 23:18:27+00:00 till 2022-08-08 23:19:24+00:00

Balloon filename (gpx)	station	expected timeframe
SMT_20220724_231539.gpx	11	2022-07-24 23:19:27+00:00 till 2022-07-24 23:21:58+00:00
SMT_20220724_231539.gpx	13	2022-07-25 00:19:35+00:00 till 2022-07-25 00:32:09+00:00
SMT_20220829_231438.gpx	22	2022-08-29 23:16:29+00:00 till 2022-08-29 23:16:42+00:00
SMT_20220829_231438.gpx	23	2022-08-29 23:17:39+00:00 till 2022-08-29 23:18:04+00:00
SMT_20220829_231438.gpx	24	2022-08-29 23:18:59+00:00 till 2022-08-29 23:19:22+00:00
SMT_20220916_231807.gpx	21	2022-09-16 23:19:09+00:00 till 2022-09-16 23:19:17+00:00
SMT_20220916_231807.gpx	22	2022-09-16 23:21:13+00:00 till 2022-09-16 23:22:03+00:00
SMT_20220816_232314.gpx	22	2022-08-16 23:33:11+00:00 till 2022-08-16 23:37:34+00:00
SMT_20220907_112500.gpx	23	2022-09-07 11:28:37+00:00 till 2022-09-07 11:28:59+00:00
SMT_20220907_112500.gpx	24	2022-09-07 11:29:35+00:00 till 2022-09-07 11:29:53+00:00
SMT_20220628_231514.gpx	12	2022-06-28 23:19:37+00:00 till 2022-06-28 23:20:55+00:00
SMT_20220630_112143.gpx	21	2022-06-30 12:21:02+00:00 till 2022-06-30 12:46:53+00:00
SMT_20220630_112143.gpx	12	2022-06-30 12:26:35+00:00 till 2022-06-30 12:48:30+00:00
SMT_20220630_112143.gpx	11	2022-06-30 12:25:33+00:00 till 2022-06-30 12:48:30+00:00
SMT_20220630_112143.gpx	13	2022-06-30 12:28:56+00:00 till 2022-06-30 12:48:30+00:00
SMT_20220630_112143.gpx	22	2022-06-30 12:23:21+00:00 till 2022-06-30 12:47:42+00:00
SMT_20220630_112143.gpx	23	2022-06-30 12:26:20+00:00 till 2022-06-30 12:47:25+00:00
SMT_20220630_112143.gpx	24	2022-06-30 12:30:34+00:00 till 2022-06-30 12:46:14+00:00
SMT_20220725_231505.gpx	21	2022-07-25 23:17:47+00:00 till 2022-07-26 00:53:39+00:00
SMT_20220725_231505.gpx	12	2022-07-26 00:38:19+00:00 till 2022-07-26 00:55:04+00:00
SMT_20220725_231505.gpx	11	2022-07-26 00:45:41+00:00 till 2022-07-26 00:55:04+00:00
SMT_20220725_231505.gpx	13	2022-07-26 00:34:56+00:00 till 2022-07-26 00:55:04+00:00
SMT_20220725_231505.gpx	22	2022-07-25 23:21:41+00:00 till 2022-07-26 00:55:04+00:00
SMT_20220725_231505.gpx	23	2022-07-25 23:25:16+00:00 till 2022-07-26 00:55:04+00:00
SMT_20220725_231505.gpx	24	2022-07-26 00:25:43+00:00 till 2022-07-26 00:55:04+00:00
SMT_20220703_111803.gpx	22	2022-07-03 11:40:24+00:00 till 2022-07-03 11:42:55+00:00
SMT_20220703_111803.gpx	23	2022-07-03 11:42:26+00:00 till 2022-07-03 11:49:33+00:00
SMT_20220703_111803.gpx	24	2022-07-03 11:45:29+00:00 till 2022-07-03 11:52:37+00:00
SMT_20220820_111609.gpx	21	2022-08-20 11:19:36+00:00 till 2022-08-20 11:21:16+00:00
SMT_20220820_111609.gpx	12	2022-08-20 11:24:02+00:00 till 2022-08-20 11:26:23+00:00
SMT_20220624_231528.gpx	12	2022-06-25 00:33:09+00:00 till 2022-06-25 00:40:51+00:00
SMT_20220624_231528.gpx	13	2022-06-25 00:28:45+00:00 till 2022-06-25 00:40:56+00:00
SMT_20220624_231528.gpx	22	2022-06-25 00:31:15+00:00 till 2022-06-25 00:34:40+00:00
SMT_20220624_231528.gpx	23	2022-06-25 00:24:52+00:00 till 2022-06-25 00:40:56+00:00
SMT_20220624_231528.gpx	24	2022-06-25 00:23:18+00:00 till 2022-06-25 00:40:56+00:00
SMT_20220701_111515.gpx	11	2022-07-01 11:21:58+00:00 till 2022-07-01 11:26:31+00:00
SMT_20220930_111518.gpx	12	2022-09-30 11:19:46+00:00 till 2022-09-30 11:20:04+00:00
SMT_20220821_111511.gpx	21	2022-08-21 12:30:15+00:00 till 2022-08-21 12:56:06+00:00
SMT_20220821_111511.gpx	12	2022-08-21 12:37:45+00:00 till 2022-08-21 12:56:06+00:00
SMT_20220821_111511.gpx	11	2022-08-21 12:37:28+00:00 till 2022-08-21 12:56:06+00:00
SMT_20220821_111511.gpx	13	2022-08-21 12:39:39+00:00 till 2022-08-21 12:56:06+00:00
SMT_20220821_111511.gpx	22	2022-08-21 12:31:58+00:00 till 2022-08-21 12:56:06+00:00
SMT_20220821_111511.gpx	23	2022-08-21 12:33:47+00:00 till 2022-08-21 12:56:06+00:00
SMT_20220821_111511.gpx	24	2022-08-21 12:39:51+00:00 till 2022-08-21 12:56:06+00:00
SMT_20220813_112235.gpx	21	2022-08-13 11:12:14+00:00 till 2022-08-13 11:12:14+00:00
SMT_20220714_231645.gpx	12	2022-07-14 23:33:22+00:00 till 2022-07-14 23:38:49+00:00
SMT_20220714_231645.gpx	11	2022-07-14 23:27:54+00:00 till 2022-07-14 23:35:34+00:00
SMT_20220714_231645.gpx	13	2022-07-14 23:37:48+00:00 till 2022-07-14 23:46:03+00:00
SMT_20220723_231622.gpx	21	2022-07-23 23:21:03+00:00 till 2022-07-23 23:30:26+00:00

Balloon filename (gpx)	station	expected timeframe
SMT_20220723_231622.gpx	21	2022-07-23 23:21:03+00:00 till 2022-07-23 23:30:26+00:00
SMT_20220723_231622.gpx	22	2022-07-23 23:30:12+00:00 till 2022-07-23 23:35:27+00:00
SMT_20220723_231622.gpx	23	2022-07-23 23:33:26+00:00 till 2022-07-23 23:37:57+00:00
SMT_20220723_231622.gpx	24	2022-07-23 23:36:33+00:00 till 2022-07-23 23:39:18+00:00
SMT_20220701_231934.gpx	22	2022-07-01 23:08:19+00:00 till 2022-07-01 23:08:19+00:00
SMT_20220701_231934.gpx	23	2022-07-01 23:08:19+00:00 till 2022-07-01 23:08:19+00:00
SMT_20220830_231921.gpx	12	2022-08-30 23:22:15+00:00 till 2022-08-30 23:22:31+00:00
SMT_20220706_231615.gpx	22	2022-07-07 00:34:24+00:00 till 2022-07-07 00:35:15+00:00
SMT_20220706_231615.gpx	23	2022-07-07 00:33:30+00:00 till 2022-07-07 00:35:15+00:00
SMT_20220706_231615.gpx	24	2022-07-07 00:33:50+00:00 till 2022-07-07 00:35:15+00:00
SMT_20220728_112143.gpx	12	2022-07-28 11:36:04+00:00 till 2022-07-28 11:38:16+00:00
SMT_20220728_112143.gpx	11	2022-07-28 11:32:06+00:00 till 2022-07-28 11:36:28+00:00
SMT_20220728_112143.gpx	13	2022-07-28 11:37:48+00:00 till 2022-07-28 11:39:49+00:00
SMT_20220716_111633.gpx	21	2022-07-16 12:05:05+00:00 till 2022-07-16 12:20:22+00:00
SMT_20220716_111633.gpx	12	2022-07-16 12:10:53+00:00 till 2022-07-16 12:24:07+00:00
SMT_20220716_111633.gpx	11	2022-07-16 12:08:23+00:00 till 2022-07-16 12:25:43+00:00
SMT_20220716_111633.gpx	22	2022-07-16 12:09:06+00:00 till 2022-07-16 12:18:35+00:00
SMT_20220715_231621.gpx	21	2022-07-16 00:08:58+00:00 till 2022-07-16 00:12:03+00:00
SMT_20220726_111605.gpx	21	2022-07-26 11:18:19+00:00 till 2022-07-26 11:19:03+00:00
SMT_20220726_111605.gpx	12	2022-07-26 12:20:14+00:00 till 2022-07-26 12:21:53+00:00
SMT_20220726_111605.gpx	13	2022-07-26 12:06:52+00:00 till 2022-07-26 12:30:56+00:00
SMT_20220726_111605.gpx	22	2022-07-26 11:21:46+00:00 till 2022-07-26 11:24:39+00:00
SMT_20220726_111605.gpx	23	2022-07-26 11:26:09+00:00 till 2022-07-26 12:22:24+00:00
SMT_20220726_111605.gpx	24	2022-07-26 11:31:17+00:00 till 2022-07-26 12:25:10+00:00
SMT_20220726_231510.gpx	11	2022-07-26 23:31:39+00:00 till 2022-07-26 23:43:04+00:00
SMT_20220724_111936.gpx	11	2022-07-24 11:24:45+00:00 till 2022-07-24 11:27:03+00:00
SMT_20220724_111936.gpx	13	2022-07-24 12:23:16+00:00 till 2022-07-24 12:33:48+00:00
SMT_20220724_111936.gpx	24	2022-07-24 12:12:44+00:00 till 2022-07-24 12:29:27+00:00
SMT_20220820_231751.gpx	13	2022-08-20 23:41:03+00:00 till 2022-08-20 23:45:01+00:00
SMT_20220820_231751.gpx	22	2022-08-20 23:39:20+00:00 till 2022-08-20 23:41:29+00:00
SMT_20220820_231751.gpx	23	2022-08-20 23:39:47+00:00 till 2022-08-20 23:42:41+00:00
SMT_20220703_231627.gpx	21	2022-07-03 23:58:58+00:00 till 2022-07-04 00:51:57+00:00
SMT_20220703_231627.gpx	12	2022-07-04 00:19:47+00:00 till 2022-07-04 00:52:09+00:00
SMT_20220703_231627.gpx	11	2022-07-04 00:19:37+00:00 till 2022-07-04 00:52:09+00:00
SMT_20220703_231627.gpx	13	2022-07-04 00:22:04+00:00 till 2022-07-04 00:52:07+00:00
SMT_20220703_231627.gpx	22	2022-07-04 00:14:09+00:00 till 2022-07-04 00:50:28+00:00
SMT_20220703_231627.gpx	23	2022-07-04 00:17:51+00:00 till 2022-07-04 00:48:29+00:00
SMT_20220703_231627.gpx	24	2022-07-04 00:23:40+00:00 till 2022-07-04 00:42:26+00:00
SMT_20220816_111548.gpx	11	2022-08-16 11:19:06+00:00 till 2022-08-16 11:20:08+00:00
SMT_20220704_231605.gpx	21	2022-07-04 23:21:14+00:00 till 2022-07-04 23:29:47+00:00
SMT_20220704_231605.gpx	22	2022-07-05 00:45:35+00:00 till 2022-07-05 00:46:21+00:00
SMT_20220704_231605.gpx	23	2022-07-05 00:44:35+00:00 till 2022-07-05 00:46:21+00:00
SMT_20220704_231605.gpx	24	2022-07-05 00:44:08+00:00 till 2022-07-05 00:46:21+00:00
SMT_20220921_231851.gpx	12	2022-09-22 10:46:18+00:00 till 2022-09-22 10:46:20+00:00
SMT_20220921_231851.gpx	13	2022-09-22 10:46:21+00:00 till 2022-09-22 10:46:22+00:00
SMT_20220630_231835.gpx	21	2022-07-01 00:11:25+00:00 till 2022-07-01 00:39:49+00:00
SMT_20220630_231835.gpx	12	2022-07-01 00:19:34+00:00 till 2022-07-01 00:45:51+00:00
SMT_20220630_231835.gpx	11	2022-07-01 00:17:35+00:00 till 2022-07-01 00:45:17+00:00

Balloon filename (gpx)	station	expected timeframe
SMT_20220630_231835.gpx	13	2022-07-01 00:23:23+00:00 till 2022-07-01 00:45:28+00:00
SMT_20220630_231835.gpx	22	2022-07-01 00:17:04+00:00 till 2022-07-01 00:40:11+00:00
SMT_20220630_231835.gpx	23	2022-07-01 00:21:11+00:00 till 2022-07-01 00:39:32+00:00
SMT_20220630_231835.gpx	24	2022-07-01 00:26:47+00:00 till 2022-07-01 00:37:45+00:00
SMT_20220807_231525.gpx	11	2022-08-07 23:18:24+00:00 till 2022-08-07 23:19:22+00:00
SMT_20220727_232120.gpx	21	2022-07-27 23:24:29+00:00 till 2022-07-27 23:25:46+00:00
SMT_20220727_232120.gpx	22	2022-07-27 23:27:22+00:00 till 2022-07-27 23:27:30+00:00
SMT_20220727_232120.gpx	23	2022-07-27 23:31:39+00:00 till 2022-07-27 23:32:39+00:00
SMT_20220727_232120.gpx	24	2022-07-27 23:33:29+00:00 till 2022-07-27 23:36:31+00:00
SMT_20220707_112434.gpx	21	2022-07-07 12:23:11+00:00 till 2022-07-07 12:49:22+00:00
SMT_20220707_112434.gpx	12	2022-07-07 12:31:06+00:00 till 2022-07-07 12:49:22+00:00
SMT_20220707_112434.gpx	11	2022-07-07 12:28:16+00:00 till 2022-07-07 12:49:22+00:00
SMT_20220707_112434.gpx	13	2022-07-07 12:34:19+00:00 till 2022-07-07 12:49:22+00:00
SMT_20220707_112434.gpx	22	2022-07-07 12:26:02+00:00 till 2022-07-07 12:49:22+00:00
SMT_20220707_112434.gpx	23	2022-07-07 12:32:01+00:00 till 2022-07-07 12:49:22+00:00
SMT_20220707_112434.gpx	24	2022-07-07 12:37:10+00:00 till 2022-07-07 12:49:22+00:00
SMT_20220617_231459.gpx	22	2022-06-17 23:17:36+00:00 till 2022-06-17 23:17:58+00:00
SMT_20220826_231852.gpx	23	2022-08-26 23:26:43+00:00 till 2022-08-26 23:28:19+00:00
SMT_20220826_231852.gpx	24	2022-08-26 23:28:41+00:00 till 2022-08-26 23:30:12+00:00
SMT_20220828_111632.gpx	22	2022-08-28 11:21:14+00:00 till 2022-08-28 11:23:09+00:00
SMT_20220828_111632.gpx	23	2022-08-28 11:24:07+00:00 till 2022-08-28 11:25:44+00:00
SMT_20220828_111632.gpx	24	2022-08-28 11:26:44+00:00 till 2022-08-28 11:28:09+00:00
SMT_20220623_231633.gpx	13	2022-06-23 23:29:11+00:00 till 2022-06-23 23:31:38+00:00
SMT_20220623_231633.gpx	22	2022-06-23 23:23:06+00:00 till 2022-06-23 23:26:51+00:00
SMT_20220807_111547.gpx	12	2022-08-07 11:22:02+00:00 till 2022-08-07 11:22:59+00:00
SMT_20220807_111547.gpx	13	2022-08-07 11:26:06+00:00 till 2022-08-07 11:27:55+00:00
SMT_20220624_111844.gpx	12	2022-06-24 11:33:01+00:00 till 2022-06-24 11:33:33+00:00
SMT_20220624_111844.gpx	13	2022-06-24 11:33:25+00:00 till 2022-06-24 11:35:11+00:00
SMT_20220624_111844.gpx	22	2022-06-24 11:31:13+00:00 till 2022-06-24 11:33:06+00:00
SMT_20220929_111540.gpx	12	2022-09-29 11:19:52+00:00 till 2022-09-29 11:20:48+00:00
SMT_20220720_111442.gpx	21	2022-07-20 11:28:20+00:00 till 2022-07-20 11:34:28+00:00
SMT_20220720_111442.gpx	22	2022-07-20 11:32:55+00:00 till 2022-07-20 11:49:29+00:00
SMT_20220720_111442.gpx	23	2022-07-20 11:37:02+00:00 till 2022-07-20 12:04:15+00:00
SMT_20220720_111442.gpx	24	2022-07-20 11:44:43+00:00 till 2022-07-20 12:12:56+00:00
SMT_20220829_111459.gpx	21	2022-08-29 11:15:53+00:00 till 2022-08-29 11:15:59+00:00
SMT_20220829_111459.gpx	23	2022-08-29 11:18:35+00:00 till 2022-08-29 11:19:05+00:00
SMT_20220829_111459.gpx	24	2022-08-29 11:19:44+00:00 till 2022-08-29 11:20:20+00:00
SMT_20220705_113009.gpx	21	2022-07-05 12:48:04+00:00 till 2022-07-05 12:53:24+00:00
SMT_20220705_113009.gpx	11	2022-07-05 12:50:13+00:00 till 2022-07-05 12:53:24+00:00
SMT_20220817_111600.gpx	21	2022-08-17 11:20:21+00:00 till 2022-08-17 11:35:09+00:00
SMT_20220817_111600.gpx	11	2022-08-17 11:27:50+00:00 till 2022-08-17 11:30:32+00:00
SMT_20220904_111459.gpx	21	2022-09-04 11:16:45+00:00 till 2022-09-04 11:18:39+00:00
SMT_20220904_111459.gpx	22	2022-09-04 11:20:46+00:00 till 2022-09-04 11:21:55+00:00
SMT_20220904_111459.gpx	23	2022-09-04 11:22:57+00:00 till 2022-09-04 11:24:53+00:00
SMT_20220904_111459.gpx	24	2022-09-04 11:24:58+00:00 till 2022-09-04 11:25:49+00:00
SMT_20220928_111604.gpx	12	2022-09-28 11:37:02+00:00 till 2022-09-28 11:38:16+00:00
SMT_20220928_111604.gpx	11	2022-09-28 11:33:16+00:00 till 2022-09-28 11:36:59+00:00
SMT_20220930_231507.gpx	13	2022-09-30 23:19:10+00:00 till 2022-09-30 23:19:35+00:00

Balloon filename (gpx)	station	expected timeframe
SMT_20220904_231730.gpx	24	2022-09-04 23:22:54+00:00 till 2022-09-04 23:23:14+00:00
SMT_20220921_111527.gpx	12	2022-09-21 11:27:31+00:00 till 2022-09-21 11:29:09+00:00
SMT_20220921_111527.gpx	11	2022-09-21 11:25:37+00:00 till 2022-09-21 11:27:09+00:00
SMT_20220921_111527.gpx	13	2022-09-21 11:29:18+00:00 till 2022-09-21 11:30:46+00:00
SMT_20220725_112511.gpx	12	2022-07-25 11:29:27+00:00 till 2022-07-25 11:30:29+00:00
SMT_20220907_231621.gpx	23	2022-09-07 23:22:59+00:00 till 2022-09-07 23:23:40+00:00
SMT_20220907_231621.gpx	24	2022-09-07 23:24:09+00:00 till 2022-09-07 23:25:07+00:00
SMT_20220827_111534.gpx	24	2022-08-27 11:22:30+00:00 till 2022-08-27 11:23:43+00:00
SMT_20220615_231713.gpx	12	2022-06-15 23:21:29+00:00 till 2022-06-15 23:22:47+00:00
SMT_20220908_111450.gpx	12	2022-09-08 11:20:02+00:00 till 2022-09-08 11:21:40+00:00
SMT_20220908_111450.gpx	13	2022-09-08 11:22:39+00:00 till 2022-09-08 11:24:21+00:00
SMT_20220616_231523.gpx	11	2022-06-16 23:17:55+00:00 till 2022-06-16 23:18:16+00:00
SMT_20220729_112533.gpx	21	2022-07-29 12:19:23+00:00 till 2022-07-29 12:33:04+00:00
SMT_20220729_112533.gpx	12	2022-07-29 12:26:18+00:00 till 2022-07-29 12:36:15+00:00
SMT_20220729_112533.gpx	11	2022-07-29 12:21:20+00:00 till 2022-07-29 12:37:29+00:00
SMT_20220704_112103.gpx	21	2022-07-04 11:46:05+00:00 till 2022-07-04 12:00:57+00:00
SMT_20220704_112103.gpx	12	2022-07-04 11:48:49+00:00 till 2022-07-04 12:35:14+00:00
SMT_20220704_112103.gpx	11	2022-07-04 11:41:27+00:00 till 2022-07-04 11:58:58+00:00
SMT_20220704_112103.gpx	13	2022-07-04 11:56:33+00:00 till 2022-07-04 12:40:36+00:00
SMT_20220704_112103.gpx	22	2022-07-04 11:49:29+00:00 till 2022-07-04 12:25:01+00:00
SMT_20220704_112103.gpx	23	2022-07-04 11:54:52+00:00 till 2022-07-04 12:33:48+00:00
SMT_20220704_112103.gpx	24	2022-07-04 11:59:40+00:00 till 2022-07-04 12:34:54+00:00
SMT_20220825_112057.gpx	12	2022-08-25 11:25:22+00:00 till 2022-08-25 11:25:43+00:00
SMT_20220712_111713.gpx	11	2022-07-12 12:29:00+00:00 till 2022-07-12 12:30:52+00:00
SMT_20220628_111612.gpx	11	2022-06-28 11:19:17+00:00 till 2022-06-28 11:19:27+00:00
SMT_20220702_231622.gpx	21	2022-07-03 00:14:37+00:00 till 2022-07-03 00:47:11+00:00
SMT_20220702_231622.gpx	12	2022-07-03 00:22:20+00:00 till 2022-07-03 00:52:30+00:00
SMT_20220702_231622.gpx	11	2022-07-03 00:29:05+00:00 till 2022-07-03 00:52:25+00:00
SMT_20220702_231622.gpx	13	2022-07-03 00:21:33+00:00 till 2022-07-03 00:52:30+00:00
SMT_20220702_231622.gpx	22	2022-07-03 00:11:26+00:00 till 2022-07-03 00:50:35+00:00
SMT_20220702_231622.gpx	23	2022-07-03 00:14:24+00:00 till 2022-07-03 00:51:28+00:00
SMT_20220702_231622.gpx	24	2022-07-03 00:16:28+00:00 till 2022-07-03 00:51:10+00:00
SMT_20220706_112237.gpx	21	2022-07-06 12:48:26+00:00 till 2022-07-06 12:48:49+00:00
SMT_20220803_232212.gpx	21	2022-08-03 23:23:53+00:00 till 2022-08-03 23:23:54+00:00
SMT_20220803_232212.gpx	22	2022-08-03 23:26:19+00:00 till 2022-08-03 23:27:55+00:00
SMT_20220803_232212.gpx	23	2022-08-03 23:29:46+00:00 till 2022-08-03 23:34:09+00:00
SMT_20220803_232212.gpx	24	2022-08-03 23:34:19+00:00 till 2022-08-03 23:38:20+00:00

BIBLIOGRAPHY

[1] Measurement of the multi-TeV neutrino interaction cross-section with IceCube using earth absorption. Nature, 551(7682):596–600, nov 2017.

[2] M. Aker, A. Beglarian, J. Behrens, A. Berlev, U. Besserer, B. Bieringer, F. Block, S. Bobien, et al. Direct neutrino-mass measurement with sub-electronvolt sensitivity. Nature Physics, 18(2):160–166, 2022.

[3] G A Askaryan. Excess negative charge of an electron-photon shower and the coherent radio emission from it. Zhur. Eksptl'. i Teoret. Fiz., 41, 8 1961.

[4] Federica Bradascio. Search for high-energy neutrinos from agn cores, 2019.

[5] Jr. Cowan, C. L., F. Reines, F. B. Harrison, H. W. Kruse, and A. D. McGuire. Detection of the Free Neutrino: A Confirmation. Science, 124(3212):103–104, July 1956.

[6] Scott Dodelson. Modern Cosmology. Academic Press, Amsterdam, 2003.

[7] K. Eguchi, S. Enomoto, K. Furuno, J. Goldman, H. Hanada, H. Ikeda, K. Ikeda, K. Inoue, et al. First results from kamland: Evidence for reactor antineutrino disappearance. Physical Review Letters, 90(2), jan 2003.

[8] Thomas K. Gaisser, Ralph Engel, and Elisa Resconi. Cosmic Rays and Particle Physics. Cambridge University Press, 2 edition, 2016.

[9] C. Glaser, D. García-Fernández, A. Nelles, J. Alvarez-Muñiz, S. W. Barwick, D. Z. Besson, B. A. Clark, A. Connolly, C. Deaconu, K. D. de Vries, J. C. Hanson, B. Hokanson-Fasig, R. Lahmann, U. Latif, S. A. Kleinfelder, C. Persichilli, Y. Pan, C. Pfendner, I. Plaisier, D. Seckel, J. Torres, S. Toscano, N. van Eijndhoven, A. Vieregg, C. Welling, T. Winchen, and S. A. Wissel. NuRadioMC: simulating the radio emission of neutrinos from interaction to detector. European Physical Journal C, 80(2):77, January 2020.

[10] C. Glaser, D. García-Fernández, A. Nelles, J. Alvarez-Muñiz, S. W. Barwick, D. Z. Besson, B. A. Clark, A. Connolly, C. Deaconu, K. D. de Vries, J. C. Hanson, B. Hokanson-Fasig, R. Lahmann, U. Latif, S. A. Kleinfelder, C. Persichilli, Y. Pan, C. Pfendner, I. Plaisier, D. Seckel, J. Torres, S. Toscano, N. van Eijndhoven, A. Vieregg, C. Welling, T. Winchen,

and S. A. Wissel. NuRadioMC: simulating the radio emission of neutrinos from interaction to detector. The European Physical Journal C, 80(2), jan 2020.

[11] Christian Glaser, Anna Nelles, Ilse Plaisier, Christoph Welling, Steven W. Barwick, Daniel García-Fernández, Geoffrey Gaswint, Robert Lahmann, and Christopher Persichilli. NuRadioReco: a reconstruction framework for radio neutrino detectors. The European Physical Journal C, 79(6), jun 2019.

[12] M. Grabe. Measurement Uncertainties in Science and Technology. Springer Berlin Heidelberg, 2005.

[13] R. Hiller, P. A. Bezyazeekov, N. M. Budnev, et al. Tunka-rex: energy reconstruction with a single antenna station. EPJ Web of Conferences, 135:01004, 2017.

[14] Tim Huege and Dave Besson. Radio-wave detection of ultra-high-energy neutrinos and cosmic rays. Progress of Theoretical and Experimental Physics, 2017(12), nov 2017.

[15] Demosthenes Kazanas. Neutrinos from AGN. In Felix A. Aharonian and Heinz J. Völk, editors, High Energy Gamma-Ray Astronomy: International Symposium, volume 558 of American Institute of Physics Conference Series, pages 370–380, April 2001.

[16] Tobias Melson, Hans-Thomas Janka, Robert Bollig, Florian Hanke, Andreas Marek, and Bernhard Müller. Neutrino-driven explosion of a 20 solar-mass star in three dimensions enabled by strange-quark contributions to neutrino–nucleon scattering. The Astrophysical Journal Letters, 808(2):L42, jul 2015.

[17] B. Oeyen, I. Plaisier, A. Nelles, C. Glaser, and T. Winchen. Effects of firn ice models on radio neutrino simulations using a RadioPropa ray tracer. In 37th International Cosmic Ray Conference. 12-23 July 2021. Berlin, page 1027, March 2022.

[18] C. Welling, P. Frank, T. Enßlin, and A. Nelles. Reconstructing non-repeating radio pulses with information field theory. Journal of Cosmology and Astroparticle Physics, 2021(04):071, apr 2021.

[19] C. Welling, C. Glaser, and A. Nelles. Reconstructing the cosmic-ray energy from the radio signal measured in one single station. Journal of Cosmology and Astroparticle Physics, 10:075–075, oct 2019.

[20] Tobias Winchen. RadioPropa — a modular raytracer for in-matter radio propagation. EPJ Web of Conferences, 216:03002, 2019.